



Australasian microtektites and associated impact ejecta in the South China Sea and the Middle Pleistocene supereruption of Toba

Billy P. GLASS^{1*} and Christian KOEBERL²

¹Geology Department, University of Delaware, Newark, Delaware 19716, USA

²Department of Geological Sciences, University of Vienna, Althanstrasse, A-1090 Vienna, Austria

*Corresponding author. E-mail: bglass@udel.edu

(Received 17 March 2005; revision accepted 22 August 2005)

Abstract—Australasian microtektites were discovered in Ocean Drilling Program (ODP) Hole 1143A in the central part of the South China Sea. Unmelted ejecta were found associated with the microtektites at this site and with Australasian microtektites in Core SO95-17957-2 and ODP Hole 1144A from the central and northern part of the South China Sea, respectively. A few opaque, irregular, rounded, partly melted particles containing highly fractured mineral inclusions (generally quartz and some K feldspar) and some partially melted mineral grains, in a glassy matrix were also found in the microtektite layer. The unmelted ejecta at all three sites include abundant white, opaque grains consisting of mixtures of quartz, coesite, and stishovite, and abundant rock fragments which also contain coesite and, rarely, stishovite. This is the first time that shock-metamorphosed rock fragments have been found in the Australasian microtektite layer. The rock fragments have major and trace element contents similar to the Australasian microtektites and tektites, except for higher volatile element contents. Assuming that the Australasian tektites and microtektites were formed from the same target material as the rock fragments, the parent material for the Australasian tektites and microtektites appears to have been a fine-grained sedimentary deposit. Hole 1144A has the highest abundance of microtektites (number/cm²) of any known Australasian microtektite-bearing site and may be closer to the source crater than any previously identified Australasian microtektite-bearing site. A source crater in the vicinity of 22° N and 104° E seems to explain geographic variations in abundance of both the microtektites and the unmelted ejecta the best; however, a region extending NW into southern China and SE into the Gulf of Tonkin explains the geographic variation in abundance of microtektites and unmelted ejecta almost as well. The size of the source crater is estimated to be 43 ± 9 km based on estimated thickness of the ejecta layer at each site and distance from the proposed source. A volcanic ash layer occurs just above the Australasian microtektite layer, which some authors suggest is from a supereruption of the Toba caldera complex. We estimate that deposition of the ash occurred ~800 ka ago and that it is spread over an area of at least 3.7 × 10⁷ km².

INTRODUCTION

Australasian tektites are found in Indochina, southern China, the Philippines, Malaysia, Indonesia, and Australia. These tektites were formed ~0.8 Ma ago based on ⁴⁰Ar/³⁹Ar dating (Izett and Obradovich 1992; Kunz et al. 1995; Yamei et al. 2000). Geochemical studies suggest that the source rock was a sedimentary deposit or rock, such as a graywacke (e.g., Taylor and Kaye 1969). The size, shape, and mineral assemblage of inclusions found in layered, or Muong Nong-type, tektites from Indochina also indicate a sedimentary source rock and suggest that it was fine-grained (Glass and Barlow 1979). Beryllium-10 studies suggest that the

Australasian tektites were derived from surface or near-surface sedimentary deposits (Pal et al. 1982; Blum et al. 1992; Ma et al. 2004). Blum et al. (1992) interpreted Sr isotopic data as indicating the source rock was Jurassic in age and proposed that the Australasian tektites may have been derived from Jurassic formations consisting of sandstone and conglomerate with interlayered micaceous shale and siltstone. On the other hand, Wasson (1991) proposed loess as the source rock.

Most investigators have concluded that the impact that produced the Australasian tektites took place somewhere in Indochina, but the source crater is still unknown (Stauffer 1978; Ford 1988; Schnetzler et al. 1988; Schnetzler 1992;

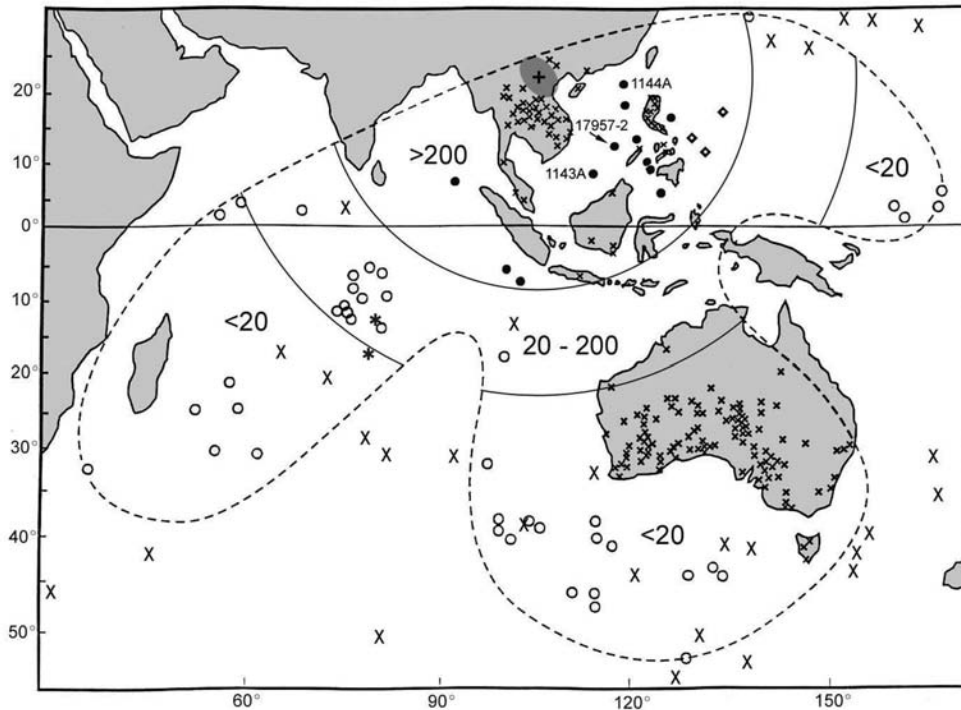


Fig. 1. Map of the Australasian tektite/microtektite strewn field. Tektite occurrences on land are indicated schematically by small “x”s. Microtektite-bearing sites in the ocean are indicated with open circles and black dots. The black dots indicate sites with the highest abundance of microtektites (number/cm²) and associated unmelted ejecta (see Table 1). Asterisk symbols indicate sites where both a tektite and microtektites have been found (Prasad and Sudhakar 1999). Marine sites where neither microtektites nor unmelted ejecta have been found are indicated with large “X”s. The apparent absence of microtektites at a given site could be due to the absence of microtektites at that site or due to searching samples from the wrong depth due to poor stratigraphic control or due to low abundance of microtektites at that site, especially near the margins of the strewn field. No microtektites were found in approximately 70 additional cores, mostly taken outside of the strewn field as defined by the dashed line. These core locations are not shown in Fig. 1 because of poor stratigraphic control and/or large sampling intervals. The known occurrences of tektites on land and microtektites in marine sites are enclosed with a dashed line that indicates the approximate limits of the strewn field as presently known. The plus sign in northern Vietnam at 22° N and 104° E indicates the location that best explains the geographic variation in abundance of unmelted ejecta and microtektites. However, anywhere within the dark gray oval, which extends from southern China through northern Vietnam into the Gulf of Tonkin, explains the geographic variation in abundance of impact ejecta and microtektites about equally well. The Australasian tektite/microtektite source crater is predicted to lie within this region. The strewn field has been divided into three regions separated by semicircles that are centered at 22° N and 104° E. Sites containing unmelted ejecta and the highest abundance of microtektites are found inside the smaller semicircle. Also shown are three sites east of the Philippines, indicated by diamonds, which contain unmelted ejecta, but no microtektites. The sites between the two semicircles have microtektite abundances between 20 and 200/cm². Beyond the outer semicircle all the sites have low microtektite abundances, <20/cm². For the latitude and longitude of and abundance of microtektites (>125 μm)/cm² in most of the microtektite-bearing sites not given in Table 1, see Glass and Pizzuto (1994).

Hartung and Koeberl 1994; Glass and Pizzuto 1994; Koeberl 1994; Lee and Wei 2000; Glass 2003; Ma et al. 2004).

Microtektites belonging to the Australasian tektite strewn field have been found in sediment cores and grab samples from nearly 60 sites throughout the Indian Ocean, western equatorial Pacific Ocean, Philippine, Sulu, and Celebes Seas, and more recently in the South China Sea (Glass et al. 1979; Peng et al. 1982; Burns 1990; Glass and Wu 1993; Glass and Pizzuto 1994; Prasad 1994; Prasad and Sudhakar 1999; Zhao et al. 1999; Lee and Wei 2000; Zhao et al. 2004; Li et al. 2005) (Fig. 1). Unmelted ejecta, such as shocked quartz with planar deformation features, coesite, and stishovite, have been found associated with the Australasian microtektites (Glass and Wu 1993). Geographic variations in concentration of microtektites and unmelted ejecta have been used to estimate

the location of the source crater, and the findings are consistent with a location in the Indochina region (Glass and Pizzuto 1994; Lee and Wei 2000).

In spite of the previous studies, the exact nature of the target rock is still being debated and the location of the source crater for the Australasian tektite/microtektite strewn field is still unknown. The main objectives of this study were to learn more about the nature of the target deposit, which was melted to form the Australasian tektites/microtektites, and to better define the location of the source crater. In order to do this, we searched for the Australasian microtektite layer and associated unmelted ejecta in cores from Ocean Drilling Program (ODP) Hole 1143A in the central part of the South China Sea, and we searched for unmelted ejecta associated with the previously described Australasian microtektite layer

in Core SO95-17957-2 (Sarnthein et al. 1994) and ODP Hole 1144A from the central and northern part of the South China Sea, respectively. These sites are closer to the more recently proposed locations for the source crater of the Australasian tektite/microtektite strewn field (e.g., Schnetzler 1992; Ma et al. 2004) than are previously studied Australasian microtektite-bearing core sites. Thus, we believed that the study of the microtektites and unmelted ejecta in these cores would give us a clearer understanding of the nature of the target rocks and location of the source crater for the Australasian strewn field.

Lee et al. (2004) described a rhyolitic volcanic ash layer, occurring just above the Australasian microtektite layer, which they propose is from an early supereruption of the Toba caldera complex in northern Sumatra. A secondary objective of the present study was to provide additional data regarding the age and geographic extent of this middle Pleistocene Toba ash layer.

CORE DATA AND METHODS

Core SO95-17957-2, hereafter referred to as Core 17957-2, was taken during a 1994 cruise of the R/V Sonne under the Sino-German cooperative project "Monitor Monsoon" (Sarnthein et al. 1994). The core was taken in a water depth of 2195 m in the central part of the South China Sea (Table 1, Fig. 1) (Sarnthein et al. 1994). ODP Hole 1143A was taken in a water depth of 2772 m and is located ~280 km southwest of where Core 17957-2 was taken (Wang, Prell, Blum et al. 2000). ODP Hole 1144A is in the northern South China Sea (Fig. 1) in a water depth of 2037 m (Wang, Prell, Blum, et al. 2000).

Samples, generally 2 to 3 cm³ in size, were taken at 1- to 3-cm intervals through the microtektite/ejecta layer and generally between 2- and 10-cm intervals above and below the layer. All samples were dried and weighed, disaggregated in water, and sieved into three size fractions (>125 μm, 63–125 μm, and <63 μm). Bioturbation is ubiquitous on the ocean floor and this has resulted in the microtektites, which were originally deposited in a layer, being reworked through a vertical section tens of centimeters or more in thickness. In order to calculate the abundance or number of microtektites that fell per unit area in a given core site, we determined the number of microtektites/cm³ at 1-cm intervals through the layer, interpolating where we did not have samples. We added the results to obtain the number per square centimeter (for more details, see Glass and Pizzuto 1994). The >125 μm size fractions were observed using a binocular microscope with up to 50× magnification and cross polarizer capability. Microtektites, mineral grains (mostly white opaque), and rock fragments were recovered and counted. X-ray diffraction (XRD) patterns were obtained, using Gandolfi and Debye-Scherrer cameras, for some randomly selected white, opaque mineral grains and rock fragments in order to document the

presence of shock-produced, high-pressure polymorphs (e.g., coesite, stishovite).

All major oxide compositions were obtained from polished sections of grain mounts. Most of the major oxide compositions presented here were determined using an ARL SEMQ electron microprobe at the Natural History Museum in Vienna (see Reimold et al. 1999 for details on instrument and methodology). The major oxide compositions of eight rock fragments were determined at the University of Delaware using an Oxford INCA energy dispersive X-ray (EDX) analyzer on a JEOL JXA-840 SEM. Because of the porosity and friability of the rock fragments, the "polished" surfaces retained some roughness. The presence of sulfur in some of the spectra (generally between 0.5 and 1 wt%) indicates that some of the voids are filled with epoxy. Sulfur was not included in the compositional data reported in this paper. Trace element contents were determined by instrumental neutron activation (INAA) analysis (see Koeberl 1993 for methodology).

During this study, and in previous searches for Australasian microtektites, the relative abundances of other components, including volcanic ash, were routinely recorded. Thus, when Lee et al. (2004) reported their findings concerning a rhyolitic volcanic ash layer just above the Australasian microtektite layer, which they attribute to an early eruption of Toba, we were able to retrieve data that allowed us to say something about the age and geographic extent of this volcanic ash layer. During this study, the relative abundance data for the ash was augmented with some size and compositional data.

All errors given in this paper are given as plus/minus one standard deviation.

RESULTS

Microtektites

Approximately 1330, 3000, and 18,190 microtektites (including fragments) were recovered from the >125 μm size fractions in Core 5H from Hole 1143A (i.e., Core 1143A-5H), Core 17957-2, and Core 37X of Hole 1144A (i.e., Core 1144A-37X), respectively. In Core 1143A-5H, the microtektites were found spread over a vertical interval of 40 cm. Microtektites were found spread over at least 225 cm in Core 17957-2, but are concentrated in a 10-cm interval between 805 and 815 cm depth. In Core 1144A-37X, the microtektites are scattered over about 81 cm, but are concentrated in a 10-cm interval. At the peak abundance, we recovered 204, 280, and 2120 microtektites per gram from Cores 1143A-5H, 17957-2, and 1144A-37X, respectively (Fig. 2).

About 36, 45, and 75% by number, of the microtektites are fragments in Cores 1143A-5H, 17957-2, and 1144A-37X, respectively. In this study, microtektites which are chipped or

Table 1. Core location, microtektite, unmelted ejecta, volcanic ash data, and estimated distance to and estimated size of the source crater.

Core/site ^a	Microtektites ^c										Unmelted ejecta ^d		Estimated crater		Assoc. vol. ash	
	Depth of peak abundance		Dist. ^b (km)	Number (>125µm)/cm ²		Fragments (%)	Depth of peak abundance (m)		Number (>125µm)/cm ²	Unmelted ejecta ^g (%)	Estimated thickness of layer ^e (cm)	Estimated crater diameter ^f (km)	vol.	ash		
	abundance (m)	abundance (m)		cm ²	abundance (m)		abundance (m)	cm ²							abundance (m)	abundance (m)
ODP 1144A	20.05° N	117.42° E	1412	345.68	9834	75	345.68	7327	43	0.17	47	no				
ODP 1143A	9.36° N	113.29° E	1717	40.26	663	36	40.26	310	31	0.01	28	yes				
17957-2	10.90° N	115.31° E	1723	8.06	2270	45	8.08	549	19	0.04	37	yes				
MD972142	12.69° N	119.56° E	1949	34.25	3199	27	n.d.	n.d.	n/a	0.03	42	n.k.				
MD972143	15.87° N	124.65° E	2279	15.71	1117	44	n.d.	n.d.	n/a	0.01	37	n.k.				
DSDP 292	15.82° N	124.65° E	2281	8.62	448	30	8.63	41	8	0.005	30	yes				
ODP 769A	8.79° N	121.22° E	2357	63.32	3196	25	63.35	111	3	0.03	49	n.k.				
ODP 758B	5.38° N	90.36° E	2358	10.96	3255	41	10.98	84	3	0.03	49	yes				
ODP 768	8.00° N	121.22° E	2414	75.61	2961	24	75.61	146	5	0.03	49	yes				
V21-125	13.68° N	128.48° E	2753	n/a	0	n/a	7.76	26	100	n.d.	n/a	n.k.				
ODP 767B	4.79° N	123.50° E	2844	49.63	2980	33	49.63	76	2	0.03	55	yes				
V19-116	11.23° N	130.17° E	3036	n/a	0	n/a	6.20	29	100	n.d.	n/a	n.k.				
V20-142	17.18° N	133.27° E	3117	n/a	0	n/a	2.70	6	100	n.d.	n/a	n.k.				
V19-153	8.85° S	102.12° E	3327	5.10	329	30	5.20	19	5	0.003	38	yes				
RC14-46	7.82° S	100.00° E	3418	9.75	1056	32	9.75	26	2	0.01	50	yes				

^aCores discussed in this paper are in bold.^bDistance from hypothetical crater site at 22° N and 104° E predicted from geographic variations in abundance of unmelted ejecta associated with the Australasian microtektite layer.^cMicrotektite data for ODP Sites 1143A and 1144A and Core 17957-2 are from this study, data for MD972142 and MD972143 are from Lee and Wei (2000), and data for the rest of the cores are from Glass and Pizzuto (1994).^dUnmelted ejecta data for ODP Sites 1143A and 1144A and Core 17957-2 are from this study and data for the rest of the cores are from Wu (1995).^eBased on estimated volume of ejecta in a one square centimeter column, an average size of 267 microns for the microtektites (Glass and Pizzuto 1994), an average size of 200 microns for the unmelted ejecta, and assumed porosity of 20% for the ejecta.^fCalculated using Stöffler et al.'s (1975) equation based on calculated layer thickness and an assumed crater location at 22° N and 104° E. This equation relates the thickness of an ejecta layer to size of and distance from the source crater.^gPercent of ejecta that was unmelted (i.e., not glass).

n/a = not applicable; n.d. = no data; n.k. = not known

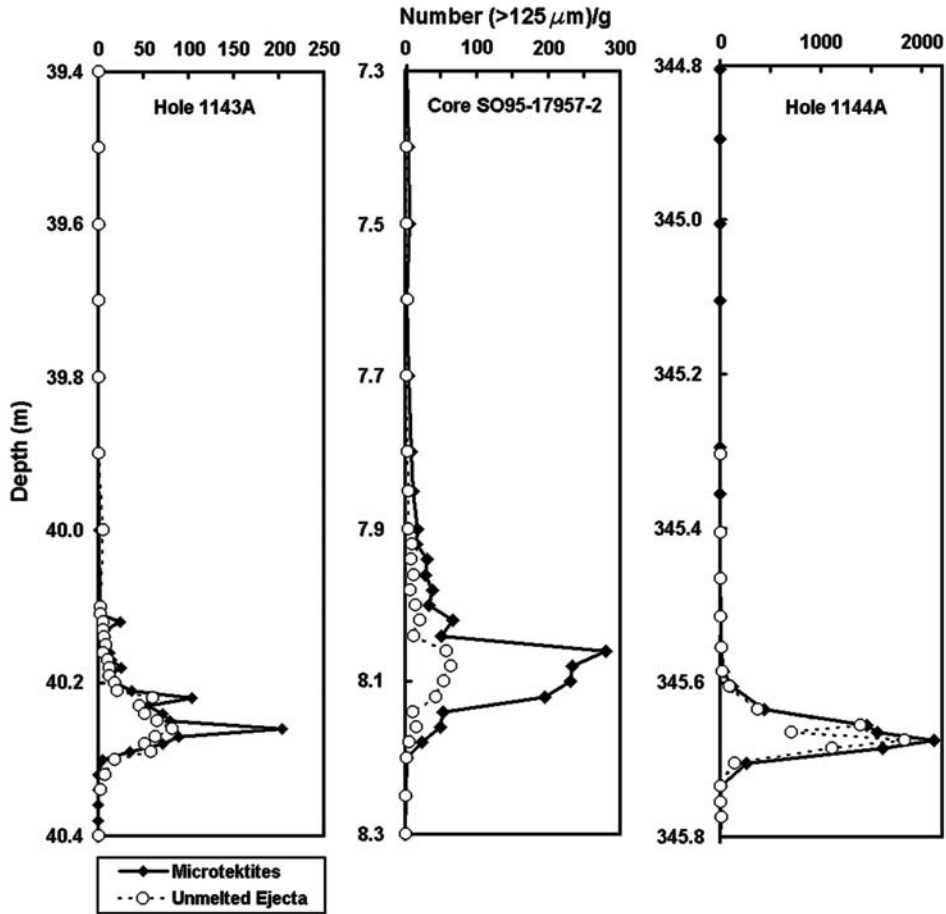


Fig. 2. Vertical distribution of microtektites and unmelted ejecta (shocked-rock and shocked-mineral grains) in Core SO95-17957-2 and ODP Holes 1143A and 1144A. Note the different horizontal scales.

broken are still defined as whole as long as more than half of the microtektite is present. Of the complete microtektites, which are primarily splash forms, most are spheroids (Fig. 3); the remainder are disk-shaped bodies, teardrops, dumbbells, cylinders, and irregular forms in decreasing order of abundance. There are a few examples of two or more splash forms fused together. The largest two recovered microtektites, both from Hole 1144A, are an oblate spheroid with a diameter of 920 μm and an elongated form with a length of 1.4 mm. The largest fragment was recovered from Core 17957-2 and it is ~ 2.1 mm in the maximum dimension. Several fragments from each site are larger than the largest microtektites from those sites and are probably tektite fragments.

Most of the microtektites and glass fragments are translucent to transparent brown in color, but pale yellow and yellow-green microtektites are also present. Pale green microtektites are rare. Many of the microtektites from Cores 17957-2 and ODP 1144A-37X have shiny, smooth surfaces, but most exhibit fine pitting and some have schlieren or flow lines etched on their surface. Most of the microtektites from Hole 1143A are deeply corroded and many have a scalloped appearance due to overlapping shallow pits. Some of the

microtektites from Hole 1144A have obvious impact pits on their surfaces. Most of the microtektites and glass fragments are vesicle free, but some contain one or two relatively large vesicles and a few are quite vesicular. The microtektites from Hole 1144A appear to be more vesicular than those from Hole 1143A and Core 17957-2. Some clear to pale yellow frothy particles were also recovered from Cores 17957-2 and ODP 1144A-37X; they appear to be more abundant at Hole 1144A.

Partly Melted Particles

A few irregular, dark, opaque, rounded, vesicular, partly melted particles were recovered from the microtektite/ejecta layer at all three sites. A large, opaque, partly melted particle, approximately 0.8×1.2 mm in size, was studied using SEM/EDS (Fig. 4). It contains large irregular vesicles up to 200 μm in length. Smaller vesicles are more spherical. The particle consists of mineral grains in a glass matrix. The most common mineral phase is quartz. The quartz grains are up to 250 μm in maximum dimension and highly fractured. K feldspar is also common and is also fractured. One large area with plagioclase composition is vesicular around its

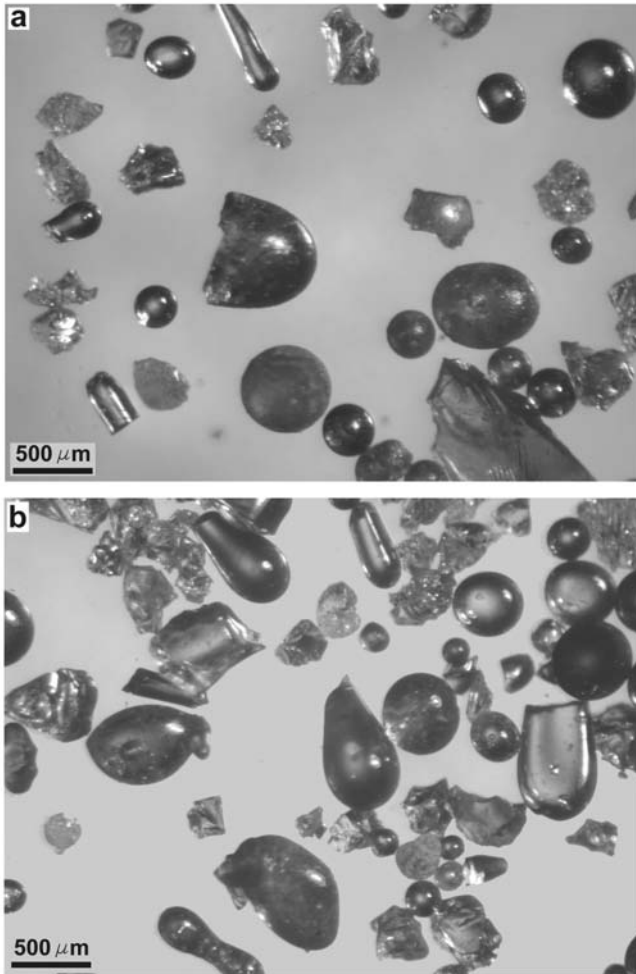


Fig. 3. An optical microscope photomicrograph of Australasian microtektites from Core SO95-17957-2 and ODP Hole 1144A. a) Australasian microtektites from the $>125\ \mu\text{m}$ size fraction from a depth of 796–797 cm in Core SO95-17957-2. Most are splash forms, but fragments are common. The splash forms are mostly spherical, but one teardrop and at least one fragment of a dumbbell are present. Note that the largest fragment is larger than any of the microtektites and may be a fragment of a tektite. b) Australasian microtektites from Core 37X, section 6, 65–66 cm from ODP Hole 1144A. Note that fragments are more abundant than the splash forms. Vesicles are obvious in some of the microtektites.

margin, indicating at least partial melting of the plagioclase. A few small zircon, rutile, and ilmenorutile grains were observed. Some of the rutile/ilmenorutile has melted to form grape-like masses, consistent with shock metamorphism (El Goresy et al. 1968).

Unmelted Ejecta

Rock and mineral fragments $>125\ \mu\text{m}$ in size are found associated with the microtektites at all three sites. The peak abundance of these grains coincides with or is within two centimeters of the peak abundance of the microtektites

(Table 1; Fig. 2). Most of the rock and mineral grains associated with the microtektites exhibit evidence of shock metamorphism, as discussed below, and thus represent unmelted impact ejecta. The percent by number of unmelted ejecta in 1143A-5H, 1144A-37X, and 17957-2 varies from 19 to 47, with the highest percentage in 1144A-37X (Table 1). The unmelted ejecta consists of rock fragments and mineral grains. Most of the mineral grains are white opaque grains, which make up 23, 44, and 46% by number of the unmelted ejecta in Cores 1144A-37X, 1143A-5H, and 17957-2, respectively. XRD data indicate that the white opaque grains at each site consist of mixtures of quartz and coesite, ranging from grains that are almost pure quartz with only a trace of coesite to grains that are almost pure coesite with only a trace of quartz. Some of the latter grains have traces of stishovite in them and one white opaque grain from Hole 1144A consists of almost pure stishovite with traces of coesite and quartz.

A grain mount was made from the 63–125 μm size fraction of the sample from Core 17957-2 with the highest number of unmelted ejecta grains per gram of sediment. Eight hundred grains were observed. Fifty quartz grains were identified. Nine or $\sim 18\%$ exhibited planar elements or a “toasted” appearance (see Short and Gold 1996; Whitehead et al. 2002), but no unambiguous planar deformation features were observed. In previous studies, we observed that shocked quartz grains are translucent to opaque white. Eight translucent to white opaque quartz grains from Core 17957-2 were mounted and studied with a petrographic microscope. None of these grains were found to contain well-defined planar deformation features, but two contained planar fractures, and two had a “toasted” appearance.

Rock fragments make up between 44 and 77% (by number) of the ejecta, with the highest percent in Hole 1144A. The rock fragments from all three cores are similar in appearance. They are all fine-grained (most grains are $<50\ \mu\text{m}$ in size) and are various shades of gray, tan, and pale green. The greenish ones appear to be micaceous. The maximum dimensions of the rock fragments are approximately 360, 440, and 600 μm from Cores 17957-2, 1144A-37X, and 1143A-5H, respectively. XRD studies of rock fragments from all three cores indicate that they are composed primarily of coesite, quartz, a mica phase (illite?), and, occasionally, stishovite (but generally only the strongest line is present). SEM/EDX analyses of five rock fragments from Core 17957-2 and thirteen rock fragments from ODP Hole 1144A indicate the presence of silica-rich phases (probably mostly quartz and coesite), K feldspar, and occasionally plagioclase (at Hole 1144A only) in a finer-grained matrix (Figs. 5 and 6). The matrix in some of the fragments appears to be micaceous. Some of the rock fragments are vesicular. The quartz/coesite and feldspar grains in the rock fragments are mostly subangular in shape.

The silica-rich ($>98\ \text{wt}\% \text{SiO}_2$) grains in many of the rock fragments from both ODP Hole 1144A and Core 17957-

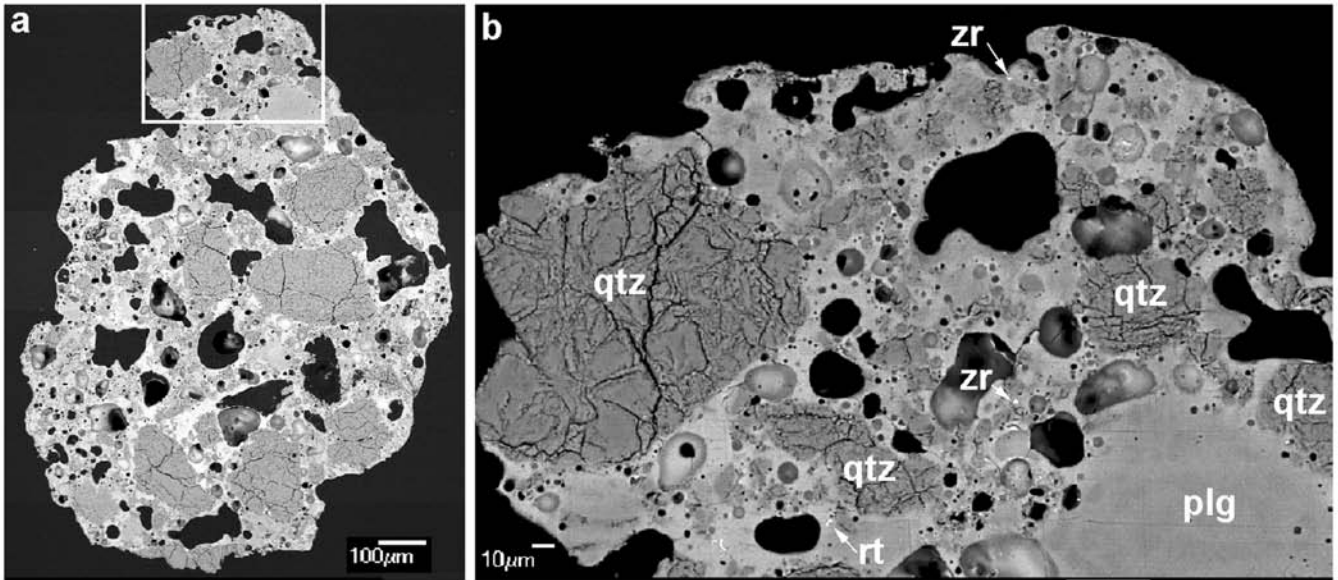


Fig. 4. BSE images of an opaque, partly-melted particle from ODP Hole 1144A, Core 37X, section 6, 60–61 cm. a) The darker gray grains are quartz. The lighter gray grains are mostly K feldspar, but some plagioclase is also present. The quartz and K-feldspar grains are subrounded to subangular and highly fractured. The plagioclase grains are vesicular around the edges, indicating incipient melting. Accessory minerals (small, bright grains) include rutile, zircon, and pyrite. Some of the rutile occurs in grape-like masses (not obvious at this magnification). The pyrite may have formed in the marine environment after deposition of the ejecta. Note the large irregular vesicles, as well as smaller spherical vesicles in the glassy matrix. b) Area outlined in (a) at higher magnification. qtz = quartz, zr = zircon, plg = plagioclase, rt = rutile.

2 have a light-colored rim surrounding a dark core in BSE images (Figs. 5b and 6). The thicknesses of the light-colored rims in a given rock fragment are fairly uniform in most cases, but vary from fragment to fragment. Occasionally, a dark core is cut through by a light-colored band, or bands, the same width as the rim (Fig. 6). In some cases there are numerous bright regions within a grain. Many of the internal bright bands or regions are associated with cracks. The boundaries between the rims and the cores are sharp. The brightness of a grain in a BSE image is determined by the average atomic number or density. Since the light-colored rims and dark cores have the same composition (SiO_2), the difference in brightness must be due to differences in density, with the bright-colored rims having a greater density than the dark cores. We suggest that the light-colored rims and interior bands and regions are coesite and the dark cores are quartz or thetomorphic quartz. This conclusion is supported by XRD data which indicate that the main phases in these rock fragments are coesite and quartz.

Observed trace minerals in the rock fragments from Core 17957-2, in approximate decreasing order of abundance, are: rutile, ilmenite, garnet, zircon, titanite, and an iron oxide phase or phases. The trace minerals are generally $<20 \mu\text{m}$ in size. A similar trace mineral assemblage was observed in the rock fragments from ODP 1144A, where the assemblage consists primarily of garnet, rutile, zircon, and ilmenite, in approximate decreasing order of abundance. One grain each of titanite, barite, apatite, and an Al_2SiO_5 phase was observed. Several grains of Ca-rich and Ca- and Mg-rich phases were

observed, which may be calcite and dolomite, respectively. Pyrite framboids are present in some of the rock fragments, but could have formed in the marine environment after deposition of the ejecta.

Composition of Glass and Rock Fragments

The major oxide contents of 15 microtektites (including one possible tektite fragment), one opaque partly melted particle, and five rock fragments from ODP Hole 1144A, were determined by electron microprobe analysis (Table 2). The trace element contents of seven of the microtektites, the partly melted particle, and the five rock fragments were determined by INAA (Table 3). The major oxide compositions of nine additional microtektites and eight additional rock fragments were determined using electron microprobe and EDX analysis, respectively (Table 2).

The microtektites and tektite fragments have similar, but somewhat different, average compositions compared to a group of 30 Australasian microtektites with similar ranges in silica contents (Table 4; Fig. 7). Although the average compositions are not the same, there is overlap in all the major oxides and trace elements except for Ba. Harker diagrams (e.g., Fig. 7) show that the microtektites and tektite fragments lie along the compositional trends of normal Australasian microtektites from 12 previously known Australasian microtektite-bearing sites, analyzed by Glass et al. (2004), although some of the microtektites in this study have lower CaO contents for a given SiO_2 content. The trace element contents are generally within a factor of two of the

Table 2. Major oxide compositions (wt%) of microtektites, a partly melted particle, and rock fragments from the Australasian microtektite layer normalized to 100 wt%.

Sample number	SiO ₂	TiO ₂	Al ₂ O ₃	FeO ^a	MnO	MgO	Microtektites ^b		CeO	Na ₂ O	K ₂ O	Total ^b	Site/core	No. ^c	Area (µm) ^d
2	68.4	0.73	14.7	5.33	0.06	2.33	2.95	2.39	3.11	100.90	ODP 1144	3	Spot		
3	74.3	0.66	12.1	4.57	0.07	4.06	2.40	0.83	1.07	99.70	ODP 1144	3	Spot		
4	64.6	0.77	18.3	6.43	0.03	2.87	2.27	1.78	2.94	100.80	ODP 1144	3	Spot		
5	64.6	0.77	17.8	6.52	0.09	2.78	1.95	2.14	3.39	100.71	ODP 1144	3	Spot		
7	67.3	0.77	15.6	5.85	0.08	2.68	3.36	1.90	2.42	100.92	ODP 1144	3	Spot		
8	65.5	0.75	17.1	6.36	0.06	2.81	2.11	2.01	3.33	99.91	ODP 1144	3	Spot		
10	72.7	0.60	11.8	4.97	0.08	2.53	2.91	2.08	2.38	100.77	ODP 1144	3	Spot		
911-1a	63.1	0.85	17.8	6.02	0.03	2.81	4.63	1.48	3.28	100.36	ODP 1144	3	Spot		
911-1b	62.9	0.85	17.3	5.96	0.05	2.82	5.31	1.67	3.19	99.84	ODP 1144	3	Spot		
911-1c	64.1	0.89	19.1	6.10	0.04	2.82	2.81	1.15	2.91	100.37	ODP 1144	3	Spot		
911-2a	62.9	0.89	18.0	7.10	0.05	3.70	2.57	1.38	3.33	100.73	17957-2	3	Spot		
911-2b	64.7	0.85	17.3	6.95	0.04	3.12	2.67	1.26	3.16	98.99	17957-2	3	Spot		
911-2c	64.7	0.82	15.9	5.84	0.02	3.64	2.51	1.97	4.54	99.07	17957-2	3	Spot		
911-3a	72.0	0.75	12.1	5.40	0.06	3.31	2.54	1.27	2.53	99.71	ODP 1143	3	Spot		
911-3b	72.5	0.73	12.0	5.40	0.04	3.18	2.51	1.21	2.43	99.53	ODP 1143	3	Spot		
911-3c	70.9	0.77	12.6	5.84	0.00	3.65	2.62	1.20	2.35	100.33	ODP 1143	3	Spot		
Ave.	67.2	0.78	15.6	5.91	0.05	3.07	2.88	1.61	2.90						
S.D.	4.0	0.08	2.6	0.68	0.02	0.48	0.89	0.45	0.74						
13 bulk	78.9	1.41	10.0	3.42	0.09	1.25	1.90	1.31	1.79	99.54	ODP 1444	5	80 × 80		
13 glass	60.8	0.53	20.5	5.60	0.23	4.20	2.47	3.18	2.48		ODP 1144	1	Spot		
1	71.4	0.47	14.7	3.95	0.04	1.27	3.48	2.02	2.68	85.73	ODP 1144	5	80 × 80		
6	62.0	1.15	22.4	7.14	0.10	2.29	0.52	1.67	2.67	85.41	ODP 1144	5	80 × 80		
9	59.3	1.24	23.2	6.35	0.06	3.09	1.96	2.48	2.42	76.31	ODP 1144	5	80 × 80		
11	72.2	0.29	15.7	3.59	0.02	1.62	2.41	1.98	2.17	55.49	ODP 1144	5	80 × 80		
12	67.3	0.74	19.7	3.97	0.06	1.37	1.75	2.17	2.89	58.48	ODP 1144	5	80 × 80		
885-1	64.7	0.71	16.3	4.76		2.21	6.89	1.04	3.31		ODP 1144	2	Variable		
885-2	66.3	0.84	15.9	5.62		2.17	5.02	1.28	2.84		ODP 1144	4	Variable		
885-3	63.3	0.89	17.5	5.54		2.23	5.88	1.37	3.23		ODP 1144	2	Variable		
885-4	66.1	0.65	17.3	6.30		2.53	2.21	1.32	3.58		ODP 1144	2	Variable		
885-5	59.2	0.68	20.3	6.56		2.90	5.66	1.26	3.49		ODP 1144	3	Variable		
885-6	73.1	0.46	14.3	3.92		1.38	2.15	2.04	2.65		ODP 1144	2	Variable		
885-7	63.9	0.46	17.9	6.13		2.65	4.49	1.11	3.34		ODP 1144	2	Variable		
885-9	70.1	0.61	15.1	5.11		2.30	2.31	1.69	2.71		ODP 1144	2	Variable		
Ave.	66.1	0.71	17.7	5.30		2.16	3.44	1.65	2.92						
S.D.	4.6	0.27	2.9	1.18		0.59	1.95	0.46	0.43						

^aAll iron reported as FeO.^bTotals prior to standardization and normalization are given for samples analyzed by electron microprobe. Compositions of samples analyzed by EDX were given as normalized to 100 wt% and were standardized and then re-normalized to 100 wt%.^cNumber of analyses made on each sample, which were then averaged.^dSize of the areas analyzed on each sample.^eSamples 2 and 4–8 could be called minitektites. Samples 2 and 4–7 are fragments of elongate forms >0.78 mm across and up to 1.25 mm long. Sample 8 is an ~1 mm diameter sphere. Sample 10 is a 0.9 × 1.05 mm angular fragment, perhaps a tektite fragment. The remainder of the microtektite samples are smaller splash-form microtektites.

Note: Samples 885-1 to 885-9 and sample 13 glass were analyzed by EDX at the University of Delaware and the Natural History Museum in Vienna, respectively. The other samples were analyzed by electron microprobe at the Natural History Museum in Vienna. A glass standard made by Corning and analyzed using wet chemistry by the U. S. Geological Survey was analyzed under the same conditions as the samples and was used to standardized the data prior to normalization to 100 wt%. Trace element contents for samples 1–13 are given in Table 3.

Table 3. K₂O and trace element compositions of microtektites, a partly melted particle, and rock fragments from ODP site 1144A determined by INAA.

Sample	Microtektites													Partly melted particle					Rock fragments				
	2	3	4	5	7	8	10	Ave.	S.D.	13	1	6	9	11	12	Ave.	S.D.						
Wt. (µg)	580.5	672.8	684.1	1066.8	570	1102	766.7			301.4	423	106.5	93.3	125.5	115.5								
K ₂ O ^a	3.19	1.08	3.01	3.45	2.41	3.35	2.41	0.83	3.95	3.22	2.70	2.70	2.61	2.72	2.21	2.69	0.36						
Sc	19.5	14.5	21.9	20.2	16.9	20.1	14.1	18.2	15.1	11.5	24.2	24.2	24.2	13.5	16.2	17.9	6.0						
Cr	123	222	127	127	105	121	185	144	109	81.9	150	150	155	77.5	117	116	36						
Co	20.3	9.61	18.3	20.7	15.3	19.8	23.9	18.3	17.0	14.7	24.9	25.9	25.7	25.7	29.5	24.1	5.6						
Ni	56	12	28	57	33	41	133	51	45	50	76	90	90	90	110	83	22						
Zn	39	1.5	9	12	13	8	38	17	24	62	186	193	193	113	120	135	55						
As	0.77	0.52	0.11	0.31	0.64	0.22	0.88	0.49	1.11	2.88	5.39	7.63	7.63	17.2	17.9	10.2	6.9						
Se	0.35	0.14	0.4	0.13	0.25	0.36	0.31	0.28	0.19	0.34	0.57	0.53	0.53	0.38	0.43	0.45	0.10						
Br	0.06	0.02	0.05	0.05	0.07	0.03	0.03	0.04	0.02	0.3	1.4	1.4	1.4	1.4	1.3	1.2	0.5						
Rb	165	48.8	161	178	129	169	120	139	131	145	114	134	134	110	126	126	14						
Zr	295	425	250	250	320	250	310	300	275	185	260	340	340	215	265	253	59						
Sb	0.44	0.053	0.11	0.34	0.27	0.26	0.44	0.27	0.15	0.40	0.70	1.63	1.23	1.05	1.07	1.14	0.34						
Cs	9.17	1.67	8.22	9.91	6.21	8.99	5.65	7.12	6.32	7.25	7.67	10.0	10.0	5.25	6.33	7.30	1.77						
Ba	328	321	349	341	325	330	291	326	315	320	334	361	361	387	420	364	40						
La	46.8	46.5	47.8	45.9	47.1	47.2	39.5	45.8	41.5	41.0	52.1	60.7	60.7	67.9	44.2	53.2	11.2						
Ce	90.5	88.3	97.5	90.5	90.6	93.6	78.7	90.0	82.2	83.2	102	119	119	129	86.4	103.9	20.0						
Nd	44.1	44.8	47.7	43.3	45.2	47.9	38.3	44.5	40.1	42.4	53.8	58.8	58.8	55.7	42.9	50.7	7.6						
Sm	7.95	7.83	8.53	7.97	8.13	8.13	7.04	7.94	7.21	7.32	8.97	10.7	10.7	10.2	7.29	8.90	1.58						
Eu	1.61	1.42	1.58	1.46	1.51	1.52	1.34	1.49	1.42	1.34	1.77	1.98	1.98	1.29	1.43	1.56	0.30						
Gd	8.33	6.94	9.21	7.11	6.66	7.65	6.24	7.45	7.66	6.56	8.72	10.2	10.2	8.38	7.50	8.27	1.37						
Tb	1.07	1.11	1.18	1.12	1.14	1.07	0.99	1.10	1.03	1.01	1.18	1.35	1.35	1.09	0.95	1.12	0.16						
Tm	0.57	0.58	0.61	0.57	0.59	0.59	0.49	0.57	0.04	0.51	0.66	0.69	0.69	0.48	0.56	0.58	0.09						
Yb	3.47	3.63	3.56	3.31	3.59	3.24	3.12	3.42	3.16	2.95	4.08	4.02	4.02	2.54	3.38	3.39	0.67						
Lu	0.54	0.54	0.57	0.53	0.56	0.55	0.51	0.54	0.52	0.48	0.57	0.61	0.61	0.40	0.56	0.52	0.08						
Hf	6.70	11.0	5.90	5.61	7.90	5.74	7.74	7.23	5.28	4.28	5.39	7.33	7.33	4.65	6.02	5.53	1.21						
Ta	1.51	1.58	1.62	1.58	1.56	1.57	1.32	1.53	1.38	1.69	1.78	1.86	1.86	1.46	1.40	1.64	0.20						
W	2.0	0.2	0.5	1.4	0.7	0.5	1.3	0.94	1.2	2.7	1.8	4.7	4.7	1.5	1.1	2.4	1.4						
Ir (ppb)	<0.5	<0.6	<0.6	0.2	<0.7	<0.5	<0.5	0.20	0.4	0.046	<0.8	0.5	0.5	<0.6	<1	0.3	0.3						
Au (ppb)	<1	0.8	0.7	0.9	1.1	0.6	0.3	0.73	0.27	0.7	0.2	1.3	1.3	1.5	1.6	1.0	0.6						
Th	18.7	17.4	21.4	19.6	22.8	20.2	15.6	19.4	16.6	14.7	22.8	26.3	26.3	35.5	16.8	23.2	8.3						
U	3.55	0.93	2.67	3.49	3.78	3.49	2.57	2.93	3.11	2.58	3.78	3.98	3.98	3.51	3.52	3.47	0.54						
K/U	7488	9677	9395	8238	5313	7999	7815	7690	10,584	10,401	5952	5465	5465	6458	5232	6457	5591						
Zr/Hf	44.0	38.6	42.4	44.6	40.5	43.6	40.1	42.0	52.1	43.2	48.2	46.4	46.4	46.2	44.0	45.6	2.0						
La/Th	2.50	2.67	2.23	2.34	2.07	2.34	2.53	2.38	2.50	2.79	2.29	2.31	2.31	1.91	2.63	2.39	0.34						
Th/U	5.27	18.7	8.01	5.62	6.03	5.79	6.07	7.93	5.34	5.70	6.03	6.61	6.61	10.1	4.77	6.64	2.05						
La _N /Yb _N	9.18	8.72	9.14	9.44	8.93	9.92	8.62	9.14	8.94	9.46	8.69	10.28	10.28	18.1	8.4	11.0	4.1						
Eu/Eu*	0.60	0.59	0.54	0.59	0.63	0.59	0.62	0.59	0.62	0.59	0.61	0.58	0.58	0.43	0.59	0.56	0.08						

^aK₂O given as wt%.

Trace elements given in ppm, except where otherwise noted.

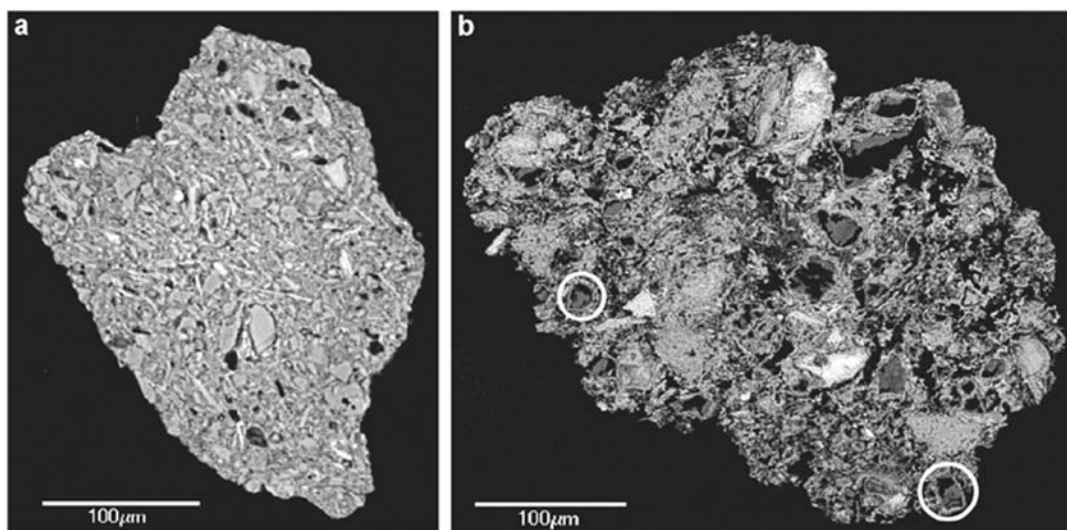


Fig. 5. BSE images of rock fragments ($>125 \mu\text{m}$) from Core SO95-17957-2, 796 cm depth. a) Most of the larger, moderate gray grains have quartz, K feldspar, and plagioclase compositions, but X-ray diffraction indicates that the most common crystalline phases are coesite and a mica, perhaps (illite?). Some of the lighter gray grains appear to be mica and amphibole/pyroxene. The smaller brighter phases include: zircon, rutile, titanite, ilmenite, and apatite. Some of the angular voids may be where grains were plucked out during polishing. b) This grain appears to be highly shocked and friable. An XRD pattern indicates that the crystalline phase in this fragment is mostly coesite with a mica. Many of the void regions may be where parts of grains were plucked out during polishing. Most of the large grains are silica with dark gray interiors and light gray borders. Two of these grains are circled. In most of these grains the dark gray interiors are partly to mostly missing and are filled with epoxy, which is black in the BSE image. Since XRD indicates that the most common crystalline phase in the grain is coesite, the light gray silica borders may be coesite and the dark gray silica interiors may be thetomorphic silica glass. Regions with K feldspar and plagioclase composition are also present; but since these minerals did not show up in the XRD pattern, they also may be thetomorphic glasses. A few of the feldspar grains are vesicular around the edges indicating some melting. Some of the brighter grains are Fe- and Mg-rich aluminum silicates and may be the mica phase (illite?) that is indicated in the XRD pattern. The accessory minerals (small, bright grains) include rutile, zircon, and garnet.

average trace element content of the upper continental crust (Table 4). The major differences are in the higher Sc, Cr, Co, Se, REE, and Th, and lower Zn, As, and Ba contents of the microtektites and tektite fragments as compared with the average upper continental crustal composition (Wedepohl 1995).

One large partly melted particle was analyzed using INAA. It has similar FeO and MnO contents compared with the microtektites/tektite fragments, but higher Na_2O and K_2O contents. However, the major oxide composition of this particle, as determined by electron microprobe analysis, falls on the compositional trends of the microtektites and rock fragments, except for the high TiO_2 (Fig. 7). The trace element contents of the partly melted particle are all within the ranges obtained for the microtektites and tektite fragments except for the Br and Hf, which are both higher (Table 3). The composition of the glassy matrix was determined by microprobe analysis. It has a low SiO_2 content ($\sim 61 \text{ wt}\%$), but is within the range for previously analyzed Australasian microtektites. The CaO and TiO_2 contents are low and the Na_2O content is high, for the SiO_2 content, compared with previously analyzed Australasian microtektites (Table 2; Fig. 7).

The major oxide content trends of the fourteen rock fragments fall on or close to those of the Australasian microtektites. The major difference is the generally lower

MgO contents of the rock fragments for a given SiO_2 content (Fig. 7). The average trace element contents of the rock fragments are within the range of the trace element contents of the microtektites, except for the volatile elements Zn, As, Br, and Sb, which are present in concentrations up to more than an order of magnitude higher than in the microtektites/tektite fragments (Tables 3 and 4). Most trace element concentrations exhibit a greater range for the rock fragments than for the microtektites, even though fewer rock fragments were analyzed. Two exceptions are the Cr and Ni contents, which have a slightly greater range in the microtektites than in the rock fragments.

Association with a Volcanic Ash Layer

We note the presence of volcanic ash just above the Australasian microtektite layer in seventeen cores in addition to the four that Lee et al. (2004) reported (Table 5; Fig. 8). In most of these cores the ash does not occur in a discrete layer, but is disseminated through a layer of sediment. The peak abundance of the ash is generally less than 15 cm above the peak abundance of the Australasian microtektites and the two layers often overlap (Table 5); however, the possible range in the difference in depth between the microtektite layer and the overlying ash layer can be rather large depending on the sampling interval.

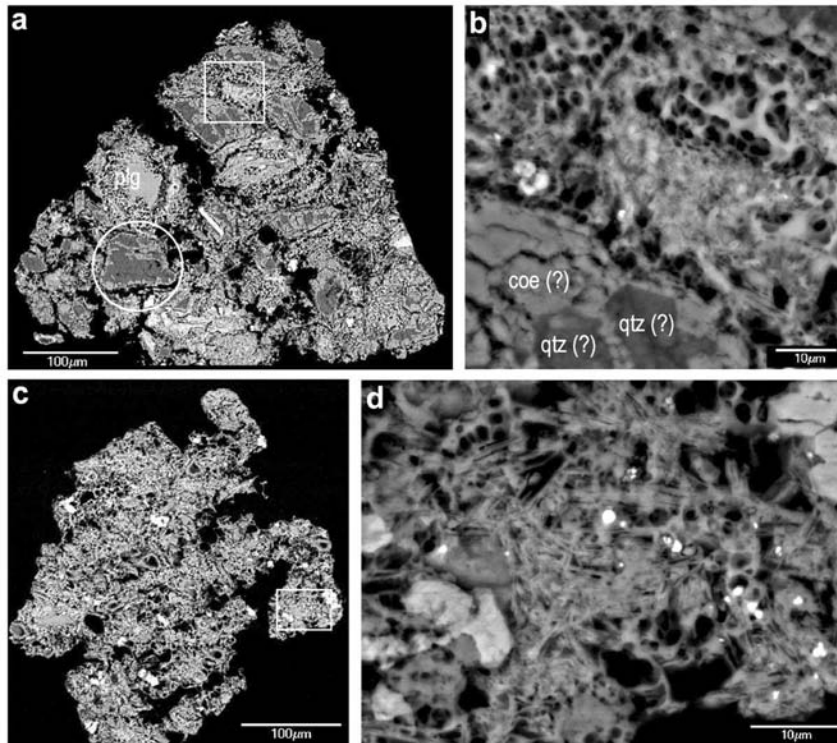


Fig. 6. BSE images of rock fragments (>125 µm in size) from ODP Hole 1144A, Core 37X, Section 6, 67–68 cm. a) Mostly dark gray rock fragment with white opaque grains, which are probably shocked quartz, based on XRD patterns of similar grains. Note the irregular margins and porosity. The larger grains with darker gray interiors and lighter gray borders are composed of silica and may be mixtures of quartz and coesite. One of these grains (in the lower left quadrant) is circled. The grain is mostly dark gray with a light gray border and a few light gray bands, which transverse the upper part of the grain. The large, light gray grain (labeled plg), in the center on the left side, is plagioclase. The outer part of the grain has melted and vesiculated. The long bright crystal near the middle is rutile. Other phases present include K feldspar, ilmenite, and perhaps biotite. b) A BSE image of the region enclosed in a square in (a). Note the vesiculation in the upper part. The lower left corner is part of a large silica grain. The darker gray regions may be quartz (qtz) and the lighter gray border and bands may be coesite (coe). c) When viewed through an optical microscope this rock fragment looked grayish green and appeared to be finely crystalline. Note the irregular shape and high porosity. The porosity is due to numerous vesicles and perhaps some voids due to plucking of grains during polishing. EDX data indicate that the main phases are silica, K feldspar, and mica. Based on X-ray diffraction studies of similar grains, the silica phases are probably coesite and quartz. The lighter gray phase may be garnet and amphibole/pyroxene. The small bright phases are trace minerals such as pyrite, rutile, and barite. d) A BSE image of the area outlined in (c). Note the platy structure which may be a mica phase, perhaps illite, which is present in these rock fragments according to XRD data. The lighter phases may be garnet. The small bright rounded grains are pyrite framboids.

We determined the major oxide compositions of the ash in ten of the cores in addition to two of the cores, 17957-2 and ODP Site 758, discussed by Lee et al. (2004). Our electron microprobe analyses indicate that the ash particles in all twelve cores have similar major oxide compositions; however, we obtained slightly higher TiO_2 , Al_2O_3 , MnO , and MgO , and somewhat lower Na_2O and K_2O contents compared with Lee et al.'s (2004) results (Table 6).

DISCUSSION

Nature of the Australasian Tektite/Microtektite Target Rock

The presence of coesite and the partial melting and vesiculation of many of the rock fragments recovered from the Australasian microtektite layer indicate that they are

impact ejecta, and their association with the Australasian microtektites (Fig. 2) indicates that they are from the Australasian tektite event. The major oxide and trace element contents of the rock fragments are similar to those of the Australasian microtektites, except for their generally lower MgO contents, for a given SiO_2 content and their higher volatile element (i.e., Zn, As, Se, Br, Sb) contents (Table 4; Figs. 7 and 9). The lower average contents of volatile elements of the tektites and microtektites, as compared to the rock fragments, may be the result of some minor vapor fractionation during tektite formation. A recent K isotope study has indicated that the Australasian microtektites experienced some evaporative losses (Herzog et al. 2005).

The trace mineral assemblage in the rock fragments is similar to that recovered from Muong Nong-type Australasian tektites. The relict mineral grains recovered from Muong Nong-type tektites are zircon, ilmenorutile, chromite, and the

Table 4. Average composition of Australasian microtektites, rock fragments from the microtektite layer, and the average upper continental crust.

	Microtektites				Rock fragments		U. cont.
	Glass et al. (2004) ^a		This study ^b		This study ^b		Crust
	Ave. (30)	S.D.	Ave. (7)	S.D.	Ave. (13)	S.D.	Ave. ^c
SiO ₂	69.1	2.68	67.2	3.99	66.1	4.60	64.92
Al ₂ O ₃	15.0	1.82	15.6	2.64	17.7	2.90	14.63
FeO ^d	5.34	0.86	5.91	0.68	5.30	1.18	3.97
MgO	3.42	0.97	3.07	0.48	2.16	0.59	2.24
CaO	3.60	0.78	2.88	0.89	3.44	1.95	4.12
Na ₂ O	0.92	0.44	1.61	0.45	1.65	0.46	3.46
K ₂ O	1.77	0.81	2.90	0.74	2.93	0.43	3.45
TiO ₂	0.82	0.07	0.78	0.08	0.71	0.27	0.52
Sc	14.6	3.2	18.2	3.0	17.9	6.0	7
Cr	147	116	144	42.5	116	36	35
Co	13.1	6.8	18.3	4.62	24.1	5.6	11.6
Ni	40	21.5	51.4	39.3	83	22	18.6
Zn	12.1	6.9	17.2	15.0	135	55	52
As	0.81	0.5	0.49	0.29	10.2	6.9	1.3
Se			0.28	0.11	0.45	0.10	0.08
Br			0.04	0.02	1.20	0.50	1.6
Rb	78	44	138	45	126	14	110
Zr	304	78	300	63	253	59	237
Sb	0.24	0.24	0.27	0.15	1.14	0.34	0.31
Cs	4.33	3.16	7.12	2.87	7.30	1.77	5.8
Ba	473	109	326	18	364	40	668
La	48.7	7.6	45.8	2.85	53.2	11.2	32.3
Ce	97.6	25.0	90.0	5.78	104	20	65.7
Nd	45.3	10.3	44.5	3.23	50.7	7.6	25.9
Sm	8.71	1.88	7.94	0.46	8.90	1.58	4.7
Eu	1.58	0.39	1.49	0.09	1.56	0.30	0.95
Gd	7.21	1.24	7.45	1.03	8.27	1.37	2.8
Tb	1.19	0.30	1.10	0.06	1.12	0.16	0.5
Tm	0.58	0.10	0.57	0.04	0.58	0.09	0.33
Yb	3.93	0.71	3.42	0.20	3.39	0.67	1.5
Lu	0.57	0.12	0.54	0.02	0.52	0.08	0.27
Hf	8.79	2.00	7.23	1.91	5.53	1.21	5.8
Ta	1.55	0.31	1.53	0.10	1.64	0.20	1.5
W	n.d.	n.d.	0.94	0.64	2.40	1.40	1.4
Ir (ppb)	<1		<0.20	<0.6	0.30	0.30	0.02
Au (ppb)	3	2	0.73	0.27	1.00	0.60	1.8
Th	15.7	4.1	19.4	2.4	23.2	8.3	10.3
U	1.74	1.31	2.93	0.99	3.47	0.54	2.5
K/U	11257	5662	7989	1434	6701	2121	11,460
Th/U	15.4	10.6	7.93	4.84	6.64	2.05	4.12
La/Th	3.28	1.00	2.38	0.20	2.39	0.34	3.14
Zr/Hf	34.9	7.1	42.0	2.3	45.6	2.0	40.9
Hf/Ta	5.81	1.19	4.74	1.30	3.40	0.71	3.87
La _N /Yb _N	8.50	1.28	9.14	0.44	11	4.1	14.7
Eu/Eu*	0.60	0.09	0.59	0.03	0.56	0.08	0.80

^aThe microtektites are from twelve different sites.^bData are from Tables 2 and 3.^cData are from Wdepohl (1995) except for values in bold, which are from Taylor and McLennan (1985).^dAll iron given as FeO.

S.D. = standard deviation.

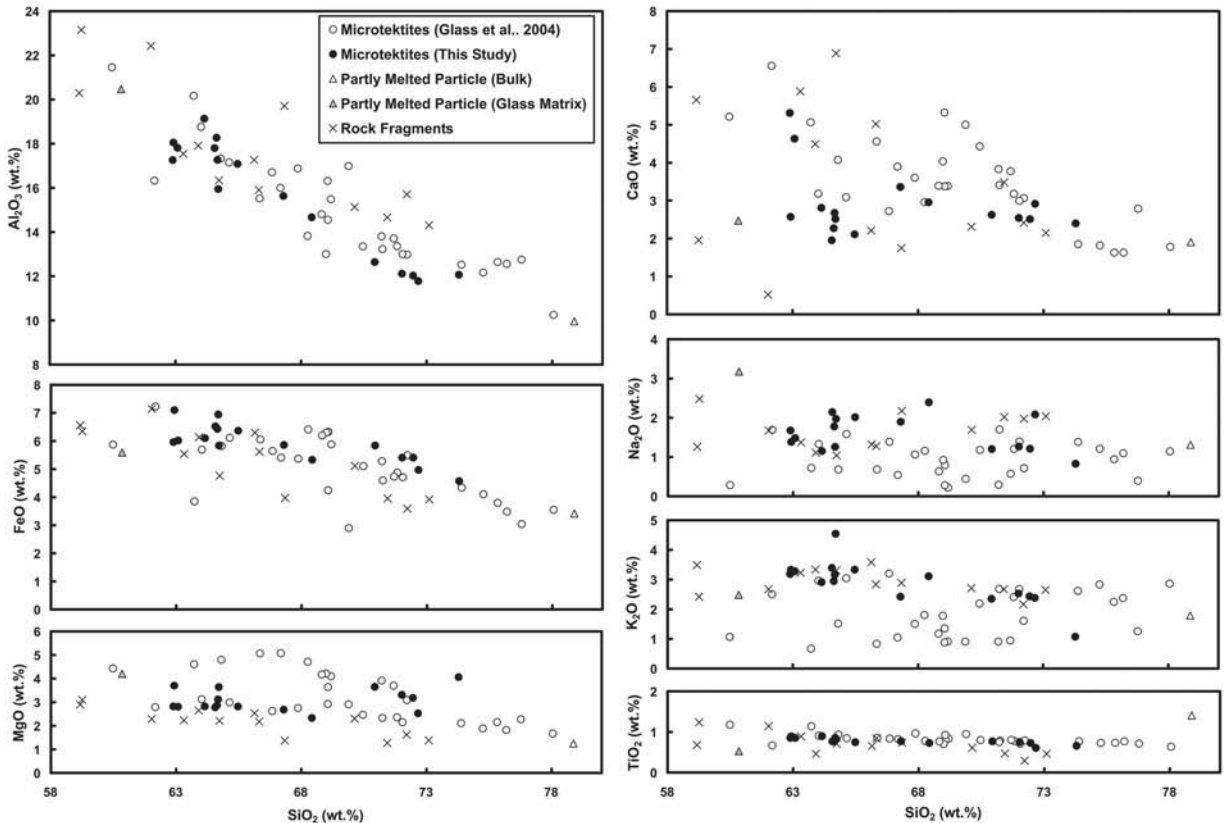


Fig. 7. Harker diagrams of Australasian microtektites from this study and from Glass et al. (2004), the glassy matrix of an opaque glassy particle, and rock fragments from ODP Hole 1144A. Note that the glassy matrix of the opaque glassy particle and rock fragments fall along or close to the compositional trends defined by the Australasian microtektites.

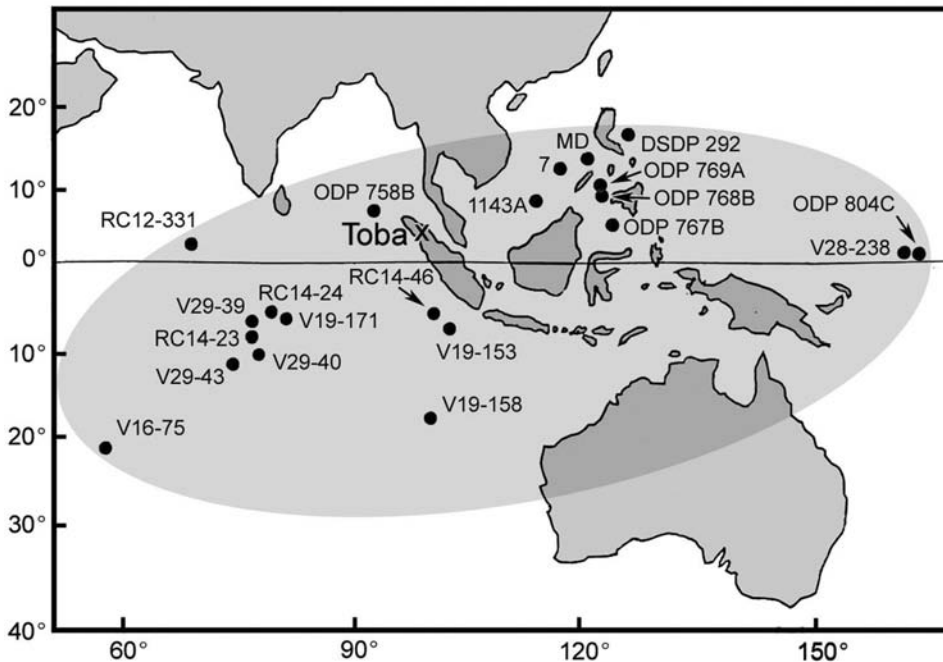


Fig. 8. A map showing location of Toba Caldera (indicated by an X) and Australasian microtektite-bearing core sites with a volcanic ash layer or disseminated ash overlapping, or just above, the microtektite layer (black dots). The geographic occurrence of this ash layer, which may be from an early eruption of the Toba volcano, is indicated by the shaded oval. The area covered by the ash layer appears to be at least 3.7×10^7 km². 1143A = ODP 1143A; 7 = Core 17957-2; MD = MD972142.

Table 5. Age difference between microtektite and volcanic ash layers.

Core ^c	Latitude	Longitude	Distance to Toba (km)	Maximum size of ash (μm)	Depth ^a		Depth difference ^b		Age difference		
					Volcanic ash layer (cm)	Microtektite layer (cm)	Min. (cm)	Max. (cm)	Sedimentation rate ^d (cm/ka)	Min (ka)	Max. (ka)
ODP 758B	5.38° N	90.36° E	985	460	1086	1093	3	11	1.36	2	8
RC14-46	7.82° S	100.00° E	1157	475	970	975	0	15	1.21	0	12
V19-153	8.85° S	102.12° E	1318	500	495	510	6	24	0.64	9	38
ODP 1143A	9.36° N	113.29° E	1779	525	4005	4026	16	26	5.01	3	5
17957-2	10.90° N	115.31° E	2054	470	803	806	1	5	1.00	1	5
V19-171	7.07° S	80.77° E	2264	390	325	340	0	30	0.42	0	71
V19-158	18.18° S	99.40° E	2288	350	33	35	0	9	0.04	0	206
RC14-24	6.62° S	79.44° E	2374	350	240	246	0	12	0.31	0	39
MD972142	12.69° N	119.56° E	2558	n.d.	3407	3425	12	24	4.27	3	6
ODP 768B	8.00° N	121.22° E	2564	420	7540	7561	12	28	9.42	1	3
ODP 769A	8.79° N	121.22° E	2584	n.d.	6310	6332	11	33	7.89	1	4
V29-39 ^e	7.70° S	77.38° E	2602	290	104	106	0	4	0.13	0	30
V29-40 ^e	20.48° S	78.05° E	2711	325	338	341	0	6	0.42	0	14
ODP 767B	4.79° N	123.50° E	2761	340	4953	4963	5	15	6.18	1	2
RC14-23	9.18° S	76.76° E	2764	330	144	144	0	6	0.18	0	33
V29-43	12.33° S	75.08° E	3095	270	433	433	0	8	0.54	0	15
DSDP 292	15.82° N	124.65° E	3203	330	850	862	0	24	1.07	0	22
RC12-331	2.50° N	69.87° E	3212	135	641	641	0	7	0.80	0	9
V16-75	22.22° S	58.38° E	5178	160	410	439	9	49	0.55	16	90
V28-238 ^f	1.02° N	160.48° E	6870	150	n.d.	1214	n.d.	n.d.	1.51	n.d.	n.d.
ODP 804C	1.00° N	161.59° E	6993	n.d.	810	820	0	28	1.02	0	27

^aDefined by the peak abundance. Ash abundances are based on a relative scale rather than actual counts.

^bThe range in depth difference between the peak abundance of the microtektites and the peak abundance (or base of a discrete ash layer) of the ash includes an error due to sampling interval, which varies from core to core.

^cCores in bold are the ones that were used to calculate the age difference between the ash and microtektite layers. Major oxide compositions of volcanic ash from cores/sites ODP 758B, RC14-46, V19-153, ODP1143A, 17957-2, V19-158, MD972142, ODP 767B, RC14-23, V29-43, DSDP 292, RC12-331, V16-75, and V28-238 can be found in Table 6.

^dCalculated by dividing depth to microtektite layer by age of the layer (assumed to be 803 ka).

^eData from Ruddiman et al. (1980).

^fAsh with the same composition as in the other cores occurs in a disseminated layer associated with the microtektite layer in this core, but there is no well-defined peak abundance.

Table 6. Major oxide composition (wt%) of volcanic ash just above the Australasian microtektite layer.

Core Sample	This work										RC14-23						
	V19-153 905-D		17957-2 905-E		ODP 767B 905-G		905-J1-J3		905-K1-K3		905-L1-L3						
SiO ₂	77.94	78.42	77.83	77.04	77.79	77.90	78.21	78.76	77.95	77.93	77.37	77.58	77.17	78.36	77.63	77.32	78.80
TiO ₂	0.22	0.15	0.17	0.13	0.10	0.13	0.15	0.05	0.30	0.18	0.26	0.20	0.22	0.05	0.17	0.11	0.10
Al ₂ O ₃	13.72	13.87	13.85	14.21	14.25	13.86	13.34	13.58	13.98	13.61	13.97	13.82	14.05	14.06	14.27	13.53	13.33
FeO	0.62	0.77	0.75	0.78	0.48	0.74	0.68	0.59	0.96	0.76	0.85	0.92	0.81	0.37	0.77	0.71	0.79
MnO	0.37	0.20	0.11	0.17	0.12	0.29	0.16	0.03	0.11	0.15	0.16	0.32	0.18	0.03	0.20	0.16	0.17
MgO	0.13	0.18	0.25	0.52	0.58	0.21	0.06	0.02	0.05	0.19	0.33	0.19	0.25	0.21	0.27	0.15	0.06
CaO	0.59	0.70	0.50	0.55	0.53	0.53	0.57	0.51	0.55	0.70	0.56	0.65	0.67	0.50	0.49	0.80	0.51
Na ₂ O	2.44	2.19	2.50	2.54	2.44	2.38	2.78	2.49	2.53	2.80	2.67	2.33	2.79	2.56	2.41	3.33	2.57
K ₂ O	3.97	3.52	4.04	4.04	3.71	3.98	4.04	3.97	3.57	3.68	3.84	3.97	3.87	3.85	3.79	3.89	3.67

Table 6. *Continued.* Major oxide composition (wt%) of volcanic ash just above the Australasian microtektite layer.

Core Sample	This work										V29-43						
	RC14-46 905-F		DSDP 292 905-H		V19-158 905-I		905-K1-K3		905-L1-L3		905-M1-M3						
SiO ₂	78.95	78.02	77.81	78.48	77.73	78.46	77.52	78.27	77.90	77.58	78.54	77.35	77.30	77.88	77.61	77.96	77.77
TiO ₂	0.05	0.08	0.21	0.04	0.23	0.12	0.07	0.15	0.15	0.18	0.06	0.37	0.24	0.13	0.14	0.07	0.16
Al ₂ O ₃	13.52	14.04	13.67	14.27	13.96	13.67	14.31	13.43	13.19	14.03	13.88	13.31	13.90	13.74	13.97	13.99	13.96
FeO	0.62	0.62	0.71	0.34	0.56	0.52	0.75	0.65	1.04	0.79	0.58	1.18	0.75	0.54	0.85	0.62	0.93
MnO	0.05	0.13	0.20	0.05	0.18	0.05	0.12	0.11	0.21	0.18	0.06	0.02	0.28	0.18	0.18	0.11	0.10
MgO	0.00	0.31	0.19	0.21	0.21	0.16	0.40	0.00	0.01	0.30	0.00	0.02	0.23	0.08	0.18	0.36	0.27
CaO	0.41	0.53	0.59	0.52	0.66	0.53	0.57	0.70	0.58	0.53	0.43	0.95	0.76	0.53	0.63	0.44	0.55
Na ₂ O	2.65	2.51	2.76	2.46	2.40	2.73	2.73	2.69	2.80	2.67	2.55	2.39	2.73	2.81	2.59	2.63	2.15
K ₂ O	3.75	3.75	3.87	3.63	4.06	3.76	3.54	4.00	4.12	3.75	3.90	3.99	3.82	4.09	3.85	3.82	4.11

Table 6. *Continued.* Major oxide composition (wt%) of volcanic ash just above the Australasian microtektite layer.

Core Sample	This work										ODP 758B		Ave.	S.D.			
	V16-75 906-A		V28-238 906-B		RC12-331 906-C		905-J4-J6		905-K1-K3		905-L1-L3						
SiO ₂	77.29	77.90	77.37	77.48	78.17	78.47	77.17	78.31	77.85	77.85	77.85	77.85	77.85	77.85	77.85	77.85	0.50
TiO ₂	0.23	0.13	0.24	0.26	0.20	0.11	0.26	0.14	0.17	0.17	0.26	0.14	0.14	0.17	0.17	0.17	0.07
Al ₂ O ₃	13.93	13.77	14.01	13.81	13.56	13.27	13.79	13.82	13.81	13.81	13.79	13.82	13.81	13.81	13.81	13.81	0.27
FeO	0.72	0.57	0.66	0.67	0.73	0.48	1.09	0.77	0.72	0.72	1.09	0.77	0.77	0.72	0.72	0.72	0.15
MnO	0.21	0.12	0.18	0.21	0.22	0.17	0.32	0.16	0.18	0.18	0.32	0.16	0.16	0.18	0.18	0.18	0.08
MgO	0.16	0.15	0.10	0.12	0.10	0.00	0.12	0.09	0.18	0.18	0.12	0.09	0.09	0.18	0.18	0.14	0.14
CaO	0.60	0.66	0.65	0.64	0.67	0.66	0.94	0.51	0.61	0.61	0.94	0.51	0.51	0.61	0.61	0.11	0.11
Na ₂ O	2.62	2.60	2.75	2.42	2.17	2.64	2.23	2.34	2.54	2.54	2.23	2.34	2.34	2.54	2.54	2.24	0.24
K ₂ O	4.24	4.09	4.04	4.39	4.17	4.20	4.10	3.84	3.94	3.94	4.10	3.84	3.84	3.94	3.94	3.84	0.21

Table 6. *Continued.* Major oxide composition (wt%) of volcanic ash just above the Australasian microtektite layer.

Core	Previous work					
	ODP 758 ^a Layer D (13)	Ave. (10)	ODP 1143 ^b S.D.	Ave. (26)	17957-2 ^b S.D.	MD972142 ^b S.D.
SiO ₂	77.75	77.74	0.27	77.87	0.36	77.80
TiO ₂	0.07	0.05	0.05	0.04	0.03	0.05
Al ₂ O ₃	12.38	12.43	0.22	12.69	0.28	12.45
FeO	0.87	0.86	0.11	0.85	0.07	0.87
MnO		0.08	0.06	0.05	0.03	0.04
MgO	0.02	0.02	0.02	0.01	0.01	0.05
CaO	0.79	0.71	0.06	0.72	0.05	0.69
Na ₂ O	2.92	3.08	0.05	2.86	0.23	2.98
K ₂ O	5.19	5.05	0.17	4.95	0.12	5.05

^aAfter Dehn et al. (1991) as reported in Lee et al. (2004).

^bLee et al. (2004)

Note: Major oxide compositions in this study were by electron microprobe at the Natural History Museum in Vienna and are normalized to 100 wt%. All iron reported as FeO. S.D. = one standard deviation.

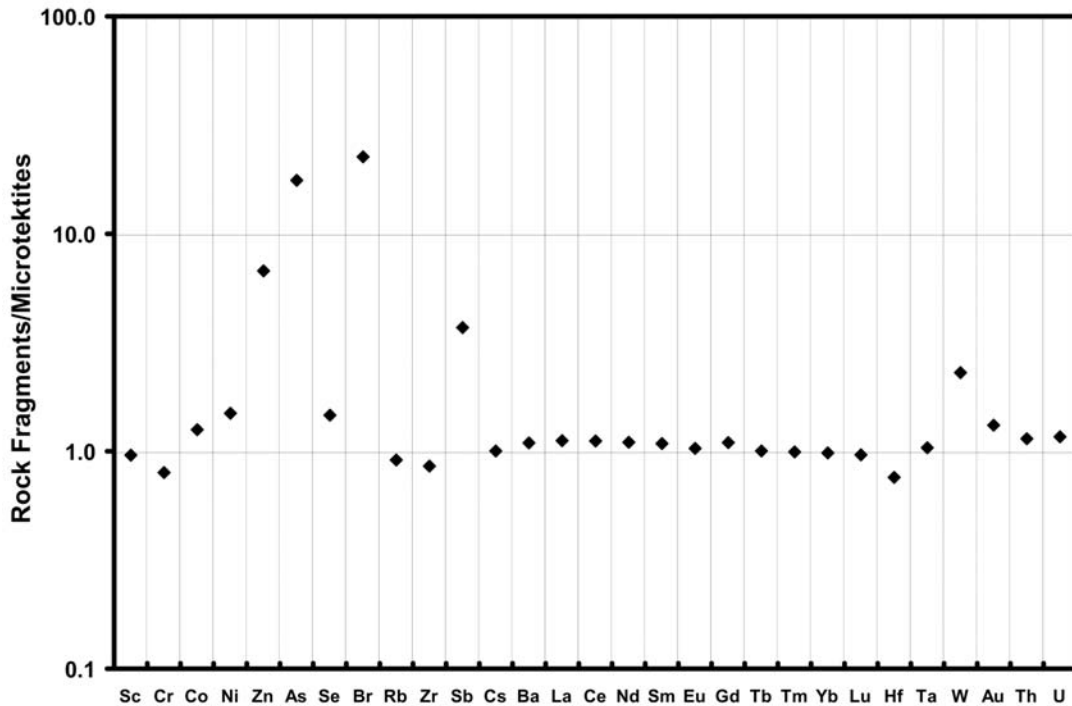


Fig. 9. Average trace element content of rock fragments (unmelted ejecta associated with the Australasian microtektite layer) normalized to the average trace element contents of the Australasian microtektites. Note that for most elements the average elemental contents of the rock fragments are within a factor of two of the average elemental contents of those elements in the microtektites. The greatest exceptions are the higher average contents of the volatile elements Zn, As, Br, and Sb in the rock fragments.

breakdown products of an Al_2SiO_5 phase (Glass and Barlow 1979). The same trace minerals, except for the chromite, occur in the rock fragments. The rock fragments also contain garnet, titanite, and a few other even rarer minerals, which may have relatively low melting temperatures and were probably destroyed during formation of the Muong Nong-type tektites. However, chromite has a high melting temperature and its apparent absence in the rock fragments poses a problem. The largest quartz grains found in the rock fragments are $\sim 100 \mu\text{m}$ across, but most are $< 50 \mu\text{m}$ in size. This size distribution appears to be consistent with the size distribution of lechatelierite particles, melted quartz, observed by Kinnunen (1990) in indochinites. Thus, it is possible that the rock fragments found in the microtektite layer represent the target deposits that were melted to produce the Australasian tektites and microtektites.

The rock fragments recovered from the Australasian microtektite layer are quartz-rich and fine-grained (Figs. 5 and 6). The grain size, texture, and mineralogy indicate a fine-grained (silt- to fine sand-sized) sedimentary target deposit. Thus, the target material could have been a fine-grained deposit from a low-energy marine environment or a fine-grained eolian deposit, e.g., loess. The rock fragments may be fragments of indurated sedimentary rocks or may be lumps of sediment welded together by shock lithification (i.e., "instant rock"; see, e.g., Short 1968). The apparent presence of calcite, dolomite, barite, and pyrite is consistent with a marine

environment, but most of these phases are rare and some could have been formed after deposition of the ejecta. In addition, no obvious nanofossils or fragments of microfossils have been observed in the rock fragments.

Loess has been suggested as the parent material for the Australasian tektites (e.g., Glass and Barlow 1979; Wasson and Heins 1993). However, based on Sr and Nd isotopic data, Blum et al. (1992) concluded that the Australasian tektite parent material was Jurassic sedimentary rock and argued against loess as the parent material. Blum et al. (1992) pointed out that Jurassic marine sedimentary rocks crop out over much of Indochina and are largely sandstones interbedded with shales and carbonates. They also pointed out that Jurassic deposits, which are exposed at the surface close to the Thailand-Laos border, are described as massive sandstone and conglomerate with interlayered micaceous shale and siltstone. The rock fragments recovered from the Australasian microtektite layer would seem to rule out a conglomerate or sandstone, unless it is a very fine-grained sandstone, as the target rock. On the other hand, the rock fragments recovered from the Australasian microtektite layer are consistent with a micaceous shale and siltstone, including loess, target rock.

Location and Size of the Source Crater

Several lines of evidence suggest that ODP Hole 1144A is closer to the source crater than any other known

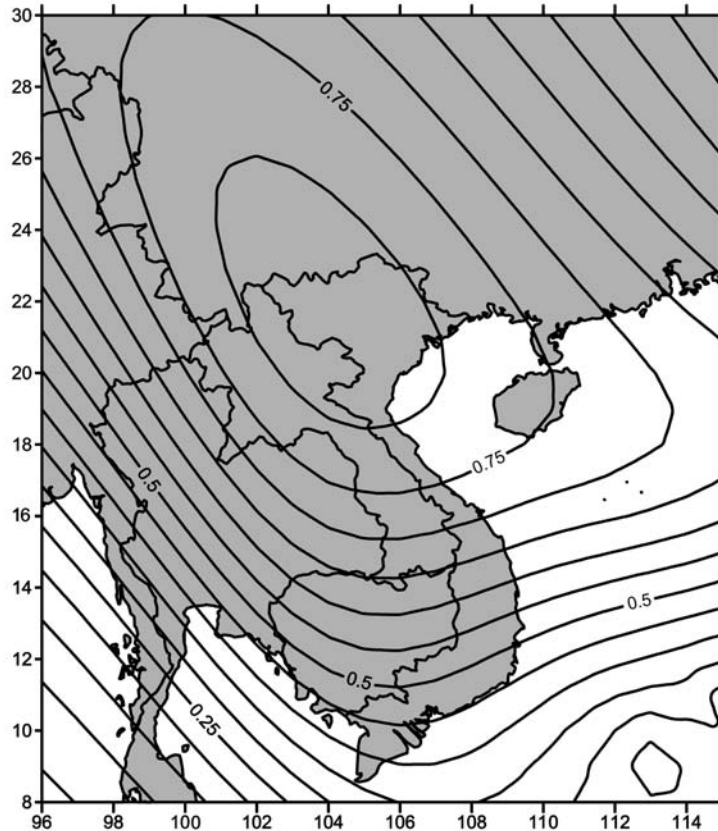


Fig. 10. Map of contoured r^2 values (total of 460). The r^2 values were obtained by calculating the distance from each location where lines of latitude and longitude intersect (at 1 degree intervals) to each site where unmelted ejecta associated with the Australasian microtektites has been found, and then performing a regression analysis of log number ($>125 \mu\text{m}/\text{cm}^2$) versus log distance. The highest r^2 value occurs at 22°N and 104°E , but anywhere within the central contour ($r^2 = 0.8$) explains the geographic variation in abundance of unmelted ejecta or microtektites nearly as well.

Australasian microtektite-bearing site. First, the microtektite concentration is three times higher than for any other known site (Table 1). Second, the ratio of unmelted ejecta (i.e., shocked-rock and mineral fragments) to melted ejecta (i.e., microtektites and tektite fragments) is the highest known for any Australasian microtektite-bearing site (Table 1). Third, the ratio of glass fragments to whole splash forms is higher than at any other site (Table 1). Previous work has shown that the number of microtektites/ cm^2 , the ratio of unmelted ejecta to melted ejecta, and the ratio of fragments to whole splash forms all increase with decreasing distance from the source crater (Glass et al. 1997). The partly melted particles have only been found associated with Australasian microtektites at sites with the highest abundance of microtektites, including ODP Hole 1144A.

Glass and Pizzuto (1994) estimated the location of the Australasian source crater using geographic variations in abundance (number $>125 \mu\text{m}/\text{cm}^2$) of Australasian microtektites (based on a method developed by Burns 1990). In this method, hypothetical crater locations are defined using the intersections of lines of latitude and longitude. At each hypothetical location, the distance to each microtektite-bearing site is determined and then a regression equation is

calculated for log abundance versus log distance. The r^2 values are calculated for each regression analysis, plotted, and then contoured to find the region that best explains the geographic variation in abundance. The location with the highest r^2 value is the predicted location of the source crater assuming that log number of microtektites and/or unmelted ejecta is negatively correlated with log distance.

Using the above method and the abundance (number $>125 \mu\text{m}/\text{cm}^2$) of microtektites for the new sites, in addition to data from the old sites with concentrations >50 microtektites ($>125 \mu\text{m}/\text{cm}^2$), the location of the source crater is predicted to be at 22°N , 104°E with an r^2 value of 0.74. The location that best explains the geographical variations in the abundance of the unmelted ejecta is the same as that for the microtektites, but the r^2 value is higher (0.83). This location is in northern Vietnam near the border with China (Fig. 10). It is much farther north ($\sim 10^\circ$) than the location predicted by Glass and Pizzuto (1994) and supported by Lee and Wei (2000). It is even farther north and west of the region proposed by Schnetzler (1992) and Ma et al. (2004) centered at 16°N and 105°E and 17°N and 107°E , respectively. However, anywhere between $\sim 25^\circ \text{N}$ and 102°E and 19°N and 106°E explains the geographic variations in the

abundance of microtektites and associated unmelted ejecta almost as well as the location at 22° N and 104° E (Fig. 10). The southeast part of this region overlaps the area in the Gulf of Tonkin, where Australasian tektites with low ^{10}Be contents have been found and which Ma et al. (2004) suggested as a possible location of the Australasian tektite source crater.

Thus, the source crater could be just off the coast of northern Vietnam in the Gulf of Tonkin. Such a location is consistent with the evidence discussed above, indicating that Site 1144A is closer to the source crater than is any other Australasian microtektite-bearing site. A crater in the Gulf of Tonkin would also explain why searches for the source crater on land have been unsuccessful (e.g., Wasson 1993; Schnetzler and McHone 1996). In addition, a crater site in this location is consistent with the ^{10}Be data of Ma et al. (2004) as discussed above. As the Australasian microtektite layer was deposited during a glacial event, oxygen isotope stage 20 (deMenocal et al. 1990; Schneider et al. 1992), much, if not most, of the Gulf of Tonkin sea floor would have been above sea level at the time of the impact, since the present water is <60 m deep.

The size of a source crater can be estimated using equations that relate the thickness of an ejecta layer to the size of, and distance from, the source crater (e.g., McGetchin et al. 1973; Stöffler et al. 1975). The abundance of the microtektites was used to estimate the thickness of the microtektite layer, prior to bioturbation, at each site. Average diameters of 267 μm and 200 μm for the microtektites (see Glass and Pizzuto 1994) and unmelted ejecta, respectively, were used in the calculations. The maximum estimated thickness of the microtektite/ejecta layer at the time of deposition, which is the greatest at ODP Hole 1144A, is only ~2 mm (Table 1). Using the estimated thicknesses from 12 sites with the highest concentration of ejecta, Stöffler et al.'s (1975) equation indicates a source crater diameter of 43 ± 9 km (1 standard deviation based on the range in estimated crater sizes) (Table 1), which is much smaller than the diameter of 99 km proposed by Lee and Wei (2000). This size estimate is based on an equation used to calculate the thickness of an ejecta blanket within a few crater diameters of the source crater. We are using it to estimate the size of a source crater that may be more than 30 crater diameters away from the closest microtektite-bearing site; thus it involves a large extrapolation. However, this method was used to estimate the size of the Ivory Coast microtektite source crater and it gave an estimated range that includes the size of Bosumtwi crater, which is believed to be the source crater for that strewn field (Glass and Pizzuto 1994). Of course, in the present case, we do not know where the source crater is and this is a major source of error. If, for example, the source crater is 100 km farther from Site 1144A than we estimated, then the size calculated for the source crater would be 50 rather than 47 km. If the crater were closer than assumed, then the estimated size would be smaller.

The Middle Pleistocene Toba Supereruption

Lee et al. (2004) proposed that rhyolitic volcanic ash found just above the Australasian microtektite layer in two cores from the South China Sea (i.e., Cores 17957-2 and MD972142) and one site from the Indian Ocean (ODP Site 758) represents dispersal from the oldest tuff associated with the Toba caldera in northern Sumatra (Fig. 8). Lee et al. (2004) traced this ash layer ~2500 km northeast of Toba (Core MD972142) and ~1000 km west northwest of Toba (ODP Site 758) (see Fig. 8) and they speculated that some of the rhyolitic ash found between ~75° and 80° E and 12° and 15° S in the central Indian Ocean may be from the same event. We have documented the presence of volcanic ash, with similar composition, just above the Australasian microtektite layer in ten additional cores (Tables 5 and 6). Our results support the presence of this ash in the central Indian Ocean and indicate that it can be found much farther to the east and west than proposed by Lee et al. (2004). We can trace it ~6900 km east of Toba into the western equatorial Pacific Ocean and as far as ~5600 km southeast of Toba (Fig. 8). We estimate that the ash layer covers an area of at least 3.7×10^7 km². This is nearly an order of magnitude larger area than documented by Lee et al. (2004). The apparent occurrence of ash from this event in two cores, V28-238 and ODP Site 804C, taken over 6800 km east of Toba in the equatorial western Pacific Ocean is difficult to explain since the prevailing winds are easterlies at this latitude. We note, however, that the ash at these two sites is fine-grained, very rare, and does not occur in a well-defined layer. In addition, we only have major oxide compositional data for the ash at one of these sites (V28-238; Table 6).

Lee et al. (2004) estimated a volume of 310–590 km³ (dense rock equivalent). At most of the additional sites the volcanic ash does not occur in a distinct layer, but is disseminated through a layer of sediment. Because our abundance data are only estimates of relative abundance, we do not have the data required to revise the volume estimate. It is likely, however, that Lee et al.'s (2004) estimate is low.

Recent dating of Australasian tektites indicates an age of $\sim 803 \pm 3$ ka for the Australasian tektite event (e.g., Yamei et al. 2000). A similar age is obtained for the Australasian microtektite layer based on an age of 789 ± 2.8 ka for the Brunhes/Matuyama (B/M) reversal boundary (Sarna-Wojcicki et al. 2000) and an age difference of ~14 ka between the Australasian microtektite layer and the B/M reversal boundary, with the Australasian microtektite layer being older (Burns 1989; Schneider et al. 1992; Lee and Wei 2000). We estimated the age difference between the Australasian microtektite layer and the ash layer at each site using sedimentation rates calculated by dividing the depth to the microtektite layer by the age of the microtektite layer (Table 5). Of course, the sedimentation rate could be different for the interval between the microtektite layer and ash layer than the average sedimentation rate calculated for the last

789 ka. Because of large sampling intervals and low apparent sedimentation rates in some cores, the range in calculated age difference is quite large. If we use the age differences only from the cores with the smaller ranges in age differences (<9 ka) and higher sedimentation rates (i.e., >0.99 cm/ka), we estimate that the ash layer is 3.4 ± 1.6 ka younger than the microtektite layer or $\sim 800 \pm 5$ ka. This age is somewhat older than the age of 788.0 ± 2.2 ka that Lee et al. (2004) obtained by extrapolation between astronomically dated (based on Milankovich cycles) oxygen isotope events 19.3 and 20.2 (from Bassinot et al. 1994) that bracket the ash layer.

SUMMARY AND CONCLUSIONS

Australasian microtektites and unmelted impact ejecta have been discovered in ODP Hole 1143A in the central part of the South China Sea, and unmelted ejecta have been discovered in the Australasian microtektite layer in Core 17957-2 and ODP Hole 1144A from the central and northern part of the South China Sea, respectively. Hole 1144A contains the highest known concentration of microtektites, ~ 9800 ($>125 \mu\text{m}$)/ cm^2 , and unmelted ejecta, ~ 7300 ($>125 \mu\text{m}$)/ cm^2 , of any known Australasian microtektite-bearing site.

Fine-grained, quartz-rich rock fragments make up a large proportion of the unmelted impact ejecta. The major and minor element contents of the rock fragments are similar to those of the Australasian microtektites and tektites, except for the more volatile elements. The porosity of the rock fragments, the grain size of the ejecta and rock fragments, and the mineral assemblage of the rock fragments, the opaque partly melted particles, and unmelted ejecta indicate that the source rock was a fine-grained, quartz-rich sedimentary deposit, possibly loess.

The high concentration of microtektites and unmelted ejecta, the high ratio of tektite and microtektite fragments to whole splash-form microtektites, and the high ratio of unmelted ejecta to microtektites (including tektite fragments) indicate that Hole 1144A is closer to the source crater than is any previously reported Australasian microtektite-bearing site. A region centered around 22° N and 104° E appears to best explain the geographic variations in abundance (number/ cm^2) of microtektites and unmelted ejecta ($>125 \mu\text{m}$ in size). However, a site off the northern coast of Vietnam would explain the geographic distribution of ejecta almost as well as a site at 22° N and 104° E and could explain why the source crater has not been found. Such a location agrees with the ^{10}Be data of Ma et al. (2004) for the Australasian tektites.

A volcanic ash layer that occurs just above the Australasian microtektite layer at 21 sites may be from a Middle Pleistocene supereruption of Toba in northern Sumatra. This ash layer appears to be about 3.2 ± 1.5 ka younger than the microtektite layer. It covers an area of at least $3.7 \times 10^7 \text{ km}^2$, which is nearly an order of magnitude larger than the area documented by Lee et al. (2004).

Acknowledgments—We thank Kevin Yezdimer for help processing the core samples from ODP Hole 1144A and for help in recovering and counting the microtektites; M. Sarthein for help in acquiring samples from Core SONNE-95-17957-2; Franz Brandstätter (Natural History Museum, Vienna), Takako Nagase and Jerry Poirier (University of Delaware) for help with microprobe and SEM, and SEM/EDX analyses, respectively. Core samples from ODP Holes 1143A and 1144A provided by the Ocean Drilling Program. C. K.'s work is supported by the Austrian Science Foundation (FWF grant P17194-N10).

Editorial Handling—Dr. John Spray

REFERENCES

- Bassinot F. C., Labeyrie L. D., Vincent E., Quidelleur X., Shackleton N. J., and Lancelot Y. 1994. The astronomical theory of climate and the age of the Brunhes-Matuyama magnetic reversal. *Earth and Planetary Science Letters* 126:91–108.
- Blum J. D., Papanastassiou D. A., Koeberl C., and Wasserburg G. J. 1992. Nd and Sr isotopic study of Australasian tektites: New constraints on the provenance and age of the target materials. *Geochimica et Cosmochimica Acta* 56:483–492.
- Burns C. A. 1989. Timing between a large impact and a geomagnetic reversal and the depth of NRM acquisition in deep-sea sediments. In *Geomagnetism and palaeomagnetism*, edited by Lowes F. J. Dordrecht: Kluwer Academic Publishers. pp. 253–261.
- Burns C. A. 1990. The Australasian microtektite layer: Implication concerning its source and relationship to the Brunhes/Matuyama geomagnetic reversal. Ph.D. thesis, University of Delaware, Newark, Delaware, USA.
- Dehn J., Farrel J. W., and Schmincke H.-U. 1991. Neogene tephrochronology from Site 758 on northern Ninetyeast Ridge: Indonesian arc volcanism for the past 5 Ma. Proceedings, Ocean Drilling Program, Scientific Results, vol. 121. pp. 273–295.
- DeMenocal P. B., Ruddiman W. F., and Kent D. V. 1990. Depth of post-depositional remanence acquisition in deep-sea sediments: A case study of the Brunhes-Matuyama reversal and oxygen isotopic stage 19.1. *Earth and Planetary Science Letters* 99:1–13.
- El Goresy A., Fechtig H., and Otterman J. 1968. The opaque minerals in impactite glasses. In *Shock metamorphism of natural materials*, edited by French B. M. and Short N. M. Baltimore: Mono Book Corporation. pp. 531–553.
- Ford R. J. 1988. An empirical model for the Australasian tektite field. *Australian Journal of Earth Sciences* 35:483–490.
- Glass B. P. 2003. Australasian microtektites in the South China Sea: Implications regarding the location and size of the source crater (abstract #1092). 34th Lunar and Planetary Science Conference. CD-ROM.
- Glass B. P. and Barlow R. A. 1979. Mineral inclusions in Muong Nong-type indochinites: Implications concerning parent material and process of formation. *Meteoritics* 14:55–67.
- Glass B. P. and Pizzuto J. E. 1994. Geographic variation in Australasian microtektite concentrations: Implications concerning the location and size of the source crater. *Journal of Geophysical Research* 99:19,075–19,081.
- Glass B. P. and Wu J. 1993. Coesite and shocked quartz discovered in the Australasian and North American microtektite layers. *Geology* 21:435–438.
- Glass B. P., Swincki M. B., and Zwart P. A. 1979. Australasian, Ivory

- Coast, and North American tektite strewn fields: Size, mass, and correlation with geomagnetic reversals and other earth events. Proceedings, 10th Lunar and Planetary Science Conference. pp. 2535–2545.
- Glass B. P., Muenow D. W., Bohor B. F., and Meeker G. P. 1997. Fragmentation and hydration of tektites and microtektites. *Meteoritics & Planetary Science* 32:333–341.
- Glass B. P., Huber H., and Koeberl C. 2004. Geochemistry of Cenozoic microtektites and clinopyroxene-bearing spherules. *Geochimica et Cosmochimica Acta* 68:3971–4006.
- Hartung J. B. and Koeberl C. 1994. In search of the Australasian tektite source crater: The Tonle Sap hypothesis. *Meteoritics* 29: 411–416.
- Herzog G. F., Alexander C. M. O'D., Glass B. P., Berger E. L., and Delaney J. S. 2005. Potassium isotope fractionation in Australasian microtektites: Evidence for evaporation and recondensation in a vapor plume (abstract #1167). 36th Lunar and Planetary Science Conference. CD-ROM.
- Izett G. A. and Obradovich J. D. 1992. Laser-fusion $^{40}\text{Ar}/^{39}\text{Ar}$ ages of Australasian tektites (abstract). 23rd Lunar and Planetary Science Conference. pp. 593–594.
- Kinnunen K. A. 1990. Lechatelierite inclusions in indochinites and the origin of tektites. *Meteoritics* 25:181–184.
- Koeberl C. 1993. Instrumental neutron activation analysis of geochemical and cosmochemical samples: A fast proven method for small sample analysis. *Journal of Radioanalytical and Nuclear Chemistry* 168:47–60.
- Koeberl C. 1994. Tektite origin by hypervelocity asteroidal or cometary impact: Target rocks, source craters, and mechanisms. In *Large impacts and planetary evolution*, edited by Dressler B. O., Grieve R. A. F., and Sharpton V. L. GSA Special Paper #293. Boulder, Colorado: Geological Society of America. pp. 133–151.
- Kunz J., Bollinger K., Jessberger E. K., and Storzer D. 1995. Ages of Australasian tektites (abstract). 26th Lunar and Planetary Science Conference. pp. 809–810.
- Lee M.-Y. and Wei K.-Y. 2000. Australasian microtektites in the South China Sea and the West Philippine Sea: Implications for age, size, and location of the impact crater. *Meteoritics & Planetary Science* 35:1151–1155.
- Lee M.-Y., Chen C.-H., Wei K.-Y., Iizuka Y., and Carey S. 2004. First Toba supereruption revival. *Geology* 32:61–64.
- Li X., Zhao Q., Huang B., and Su X. 2005. High-resolution age estimation of the mid-Pleistocene impact event. *Marine Geology and Quaternary Geology* 24:73–77. In Chinese.
- Ma P., Aggrey K., Tonzola C., Schnabel C., de Nicola P., Herzog G. F., Wasson J. T., Glass B. P., Brown L., Tera F., Middleton R., and Klein J. 2004. Beryllium-10 in Australasian tektites: Constraints on the location of the source crater. *Geochimica et Cosmochimica Acta* 68:3883–3896.
- McGetchin T. R., Settle M., and Head J. W. 1973. Radial thickness variation in impact crater ejecta: Implications for lunar basin deposits. *Earth and Planetary Science Letters* 20:226–236.
- Pal D. K., Tuniz C., Moniot R. K., Kruse T. H., and Herzog G. F. 1982. Beryllium-10 in Australasian tektites: Evidence for a sedimentary precursor. *Science* 218:787–789.
- Peng H., Zhao K., and Chen S. 1982. The evidence for 'CHO1' in sediment core samples of the Pacific Ocean collected among FGGE. *Journal of Geophysical Research* 87:5563–5565.
- Prasad M. S. 1994. New occurrences of Australasian microtektites in the Central Pacific Basin. *Meteoritics* 29:66–69.
- Prasad M. S. and Sudhakar M. 1999. Australasian minitektites discovered in the Indian Ocean. *Meteoritics & Planetary Science* 34:179–184.
- Reimold W. U., Koeberl C., Brandstätter F., Kruger F. J., Armstrong R. A., and Bootsman C. 1999. The Morokweng impact structure, South Africa: Geological, petrological, and isotopic results, and implications for the size of the structure. In *Large meteorite impacts and planetary evolution II*, edited by Dressler B. O. and Sharpton V. L. GSA Special Paper #339. Boulder, Colorado: Geological Society of America. pp. 61–90.
- Ruddiman W. F., Jones G. A., Peng T.-H., Glover L. K., Glass B. P., and Liebertz P. J. 1980. Tests for size and shape dependency in deep sea mixing. *Sedimentary Geology* 25:257–276.
- Sarna-Wojcicka A. M., Pringle M. S., and Wijbrans J. 2000. New age of the Bishop Tuff from multiple sites and sediment rate calibration for the Matuyama-Brunhes boundary. *Journal of Geophysical Research* 105 (B9):21,431–21,443.
- Sarnthein M., Pflaumann U., Wang P., and Wong H.-K., eds. 1994. Preliminary report on Sonne-95 cruise "Monitor Monsoon" to the South China Sea. In *Berichte Reports* 68. Kiel: Geologisch-Paläontologisches Institut, Universität Kiel, Germany. 225 p.
- Schneider D. A., Kent D. V., and Mello G. A. 1992. A detailed chronology of the Australasian impact event, the Brunhes-Matuyama geomagnetic polarity reversal, and global climate change. *Earth and Planetary Science Letters* 111:395–405.
- Schnetzler C. C. 1992. Mechanism of Muong Nong-type tektite formation and speculation on the source of the Australasian tektites. *Meteoritics* 27:154–165.
- Schnetzler C. C. and McHone J. F. 1996. Source of Australasian tektites: Investigating possible impact sites in Laos. *Meteoritics & Planetary Science* 31:73–76.
- Schnetzler C. C., Walter L. S., and Marsh J. G. 1988. Source of the Australasian tektite strewn field: A possible impact site. *Geophysical Research Letters* 15:357–360.
- Short N. M. 1968. Experimental microdeformation of rock material by shock pressures from laboratory-scale impacts and explosions. In *Shock metamorphism of natural materials*, edited by French B. M. and Short N. M. Baltimore: Mono Book Corporation. pp. 219–253.
- Short N. M. and Gold D. P. 1996. Petrography of shocked rocks from the central peak at the Manson impact structure. In *The Manson impact structure, Iowa: Anatomy of an impact crater*, edited by Koeberl C. and Anderson R. R. GSA Special Paper #302. Boulder, Colorado: Geological Society of America. pp. 245–265.
- Stauffer P. H. 1978. Anatomy of the Australasian tektite strewnfield and the probable site of its source crater. Proceedings, 3rd Regional Conference on Geology and Mineral Resources of Southeast Asia, Bangkok. pp. 285–289.
- Stöffler D., Gault D. E., Wedekind J., and Polkowski G. 1975. Experimental hypervelocity impact into quartz sand: Distribution and shock metamorphism of ejecta. *Journal of Geophysical Research* 80:4062–4077.
- Taylor S. R. and Kaye M. 1969. Genetic significance of the chemical composition of tektites: A review. *Geochimica et Cosmochimica Acta* 33:1083–1100.
- Taylor S. R. and McLennan S. M. 1985. *The continental crust: Its composition and evolution*. Oxford: Blackwell Scientific Publication. 312 p.
- Wang P., Prell W. L., Blum P., et al. 2000. Proceedings, Ocean Drilling Program, Initial Reports, vol. 184. CD-ROM.
- Wasson J. T. 1991. Layered tektites: A multiple impact origin for the Australasian tektites. *Earth and Planetary Science Letters* 102: 95–109.
- Wasson J. T. 1993. The search for small craters that produced the Australasian layered tektites (abstract). *EOS Transactions* 75(43):409.
- Wasson J. T. and Heins W. A. 1993. Tektites and climate. *Journal of Geophysical Research* 98:3043–3052.
- Wedepohl K. H. 1995. The composition of the continental crust. *Geochimica et Cosmochimica Acta* 59:1217–1232.

- Whitehead J., Spray J. G., and Grieve R. A. F. 2002. The origin of "toasted" quartz in terrestrial impact structures. *Geology* 30:431–434.
- Wu J. 1995. Studies of impact ejecta associated with the Australasian microtektites in deep-sea sediments: Implications concerning the source region of the Australasian tektite strewn field. Ph.D. thesis, University of Delaware, Newark, Delaware, USA.
- Yamei H., Potts R., Baoyin H., Zhengtang G., Dieno A., Wei W., Clark J., Guangmao X., Weiwen H. 2000. Mid-Pleistocene Acheulean-like stone technology of the Bose Basin, South China. *Science* 287:1622–1626.
- Zhao Q., Jian Z., Li B., Cheng X., and Wang P. 1999. Microtektites in the Middle Pleistocene deep-sea sediments of the South China Sea. *Science in China (Series D)* 42:531–535.
- Zhao Q., Jian Z., Cheng X., Liu Z., Xu J., and Xia P. 2004. Mid-Pleistocene impact and marine environmental changes: a high-resolution record from ODP site, South China Sea. *Acta Micropaleontologica Sinica* 21:130–135. In Chinese.
-